WARWICK
THE UNIVERSITY OF WARWICK

Original citation:
Mirodatos, C., Van Veen, Andre C., Pokrovskaya, S. A., Chumakova, N. A., Sazonova, N. N. and Sadykov, V. A. (2018) Modeling of transient studies on the reaction kinetics over catalysts with lattice oxygen mobility : dry reforming of CH 4 over a Pt/PrCeZrO catalyst. Chemical Engineering Journal, 343 . pp. 530-543. doi:10.1016/j.cej.2018.03.037

Permanent WRAP URL:
http://wrap.warwick.ac.uk/101767

Copyright and reuse:
The Warwick Research Archive Portal (WRAP) makes this work by researchers of the University of Warwick available open access under the following conditions. Copyright © and all moral rights to the version of the paper presented here belong to the individual author(s) and/or other copyright owners. To the extent reasonable and practicable the material made available in WRAP has been checked for eligibility before being made available.

Copies of full items can be used for personal research or study, educational, or not-for-profit purposes without prior permission or charge. Provided that the authors, title and full bibliographic details are credited, a hyperlink and/or URL is given for the original metadata page and the content is not changed in any way.

Publisher's statement:
© 2018, Elsevier. Licensed under the Creative Commons Attribution-NonCommercial-NoDerivatives 4.0 International http://creativecommons.org/licenses/by-nc-nd/4.0/

A note on versions:
The version presented here may differ from the published version or, version of record, if you wish to cite this item you are advised to consult the publisher's version. Please see the 'permanent WRAP url' above for details on accessing the published version and note that access may require a subscription.

For more information, please contact the WRAP Team at: wrap@warwick.ac.uk

warwick.ac.uk/lib-publications

*Revised Manuscript (clean for typesetting)
Click here to view linked References

Modeling of transient studies on the reaction kinetics over catalysts with lattice oxygen mobility: Dry reforming of CH_4 over a Pt/PrCeZrO catalyst

C. Mirodatos[a], A. C. van Veen[b], S. A. Pokrovskaya[c,d], N. A. Chumakova[c,d], N. N. Sazonova[c], V. A. Sadykov[c,d,*]

[a]*Institut de Recherches sur la Catalyse et l'Environnement de Lyon, Lyon, France*

[b]*University of Warwick, School of Engineering, Coventry CV4 7AL, United Kingdom*

[c]*Boreskov Institute of Catalysis SB RAS, 630090 Novosibirsk, Russia*

[d]*Novosibirsk State University, 630090 Novosibirsk, Russia*

Abstract

Dynamics of red-ox reactions occurring over catalysts with active oxide support is described by mathematical modeling. Numerical analysis is applied to transients from an initially oxidized state of a Pt/PrCeZrO catalyst to a partially reduced steady state present during CH_4 dry reforming. Oxygen transport to the surface from adjacent regions in the catalyst lattice is considered to quantify the impact on the transient behavior in the model red-ox reaction over the catalyst with a high lattice oxygen mobility. Chemical transformations and coverages at the catalyst surface are largely affected by the internal transport of oxygen species, while the overall character and shape of transient curves remain defined by the specificity of the reaction kinetic scheme.

Detailed analysis of CH_4 dry reforming over a Pt/PrCeZrO catalyst at contact times of 4.7, 8, and 15 ms allowed to (1) clarify the factors that control dynamic system behavior and catalytic properties, (2) discriminate kinetic schemes, (3) confirm a high efficiency of cationic Pt species in CH_4 dissociation, and (4) underpin that CO_2 transformation may occur via carbonate intermediates located on oxidized Pt^{n+}-Pr^{4+}-O surface sites. Direct estimation of bulk oxygen diffusion rate as well as kinetic parameters was carried out. Findings are consistent with the

characteristics of the catalyst surface state and oxygen mobility in the surface/bulk layers.

Keywords: transient studies, kinetic modeling, lattice oxygen mobility, active oxide support, CH_4 dry reforming, Pt promoted catalyst.

**Corresponding author: Prof. V. A. Sadykov, tel: +7-383-326-9541; fax: +7-383-330-8056*

E-mail address: sadykov@catalysis.ru

1. Introduction

Transient methods for studying the catalytic reaction kinetics are known to be much more efficient than the conventional steady-state approaches in revealing some specific features of a reaction mechanism and providing information about the intrinsic reaction kinetics with considerable reduction of the number of experimental runs and time consumed. Development of the computational tools for transient kinetic investigation in combination with the experimental studies permits to obtain more information about the catalyst surface state and the reaction rates. As a result, the kinetic data required for the reactor design and process optimization are elucidated. These approaches have been applied successfully to the gas-solid systems where the catalytic properties are mainly controlled by the chemical transformations at the catalyst surface [1-10].

The character of transients of a complex catalytic reaction depends on the processes that determine the alterations of the catalytic surface. Besides the chemical reaction stages, some physical processes such as the surface and bulk diffusion could influence the surface state. These processes have different time scales, and their impact on transient behavior of the system can be rather complex. A number of studies have revealed that for the oxide catalysts the bulk oxygen mobility can play an important role in the system dynamics [4, 10-16]. Near-surface oxygen mobility of solid catalysts strongly affects not only the character of transient regimes, but activity, selectivity, and stability of the catalysts performance because the surface state and, respectively, the reaction rates are determined both by transformations of the reactive surface species and the oxygen transport to the surface from the bulk layers of catalyst particle.

For example, the impact of oxygen mobility on the catalyst properties was studied for nanocrystalline Pt/LnCeZrO catalysts doped with rare-earth elements (Ln = Gd, Pr, La) in partial oxidation of methane, methane steam/dry reforming, and autothermal reforming of acetone into syngas [14-24]. Due to strong interaction of supported Pt with doped ceria-zirconia oxides, after pretreatment of catalysts in O_2 it is mainly present as Pt^{2+} and Pt^{4+} cations (XPS data [18])

possessing a high ability to activate CH_4 as revealed by TAP (Temporal Analysis of Products) [20] and transient [14, 16, 19, 20] studies. It was shown that the bulk oxygen mobility is important for stable performance of these catalysts in the frame of the bifunctional reaction mechanism. In this case, the fuel molecules are activated on the Pt sites producing $C_xH_yO_z$ species, while the molecules of oxidants dissociate on the partially reduced sites of the support producing reactive oxygen species. The latter rapidly migrate to Pt sites via the surface/near-surface diffusion and consume $C_xH_yO_z$ species thus producing syngas and preventing coking. The rates of near-surface (as well as along domain boundaries) or bulk oxygen diffusion estimated for doped ceria-zirconia oxides with supported Pt by analysis of the oxygen isotope exchange data/chemical transients are high enough (oxygen diffusion coefficients D_V in the range of $10^{-12}\div10^{-14}$ cm^2/s at 600-700 ^oC [14-16, 24-27]) to provide the required rates of oxygen transfer to the metal-support interface.

Experiments with single channels of honeycomb corundum substrate loaded with these active components (gas stream contacted only with the internal part of the channel) were carried out to elucidate dynamics of the catalysts interaction with reaction media, basic features of mechanism and kinetics of these reactions [16, 17, 19-23, 28, 29]. Similar to the well-known approach based on the annular reactor design [30], these experiments with single channels allowed to minimize the impact of heat- and mass transfer on kinetic transients, thus providing reliable data on the main features of reaction mechanism and kinetics. On the bases of these experiments, $Pt/Pr_{0.3}Ce_{0.35}Zr_{0.35}O_x$ active component was selected as the most promising for detailed studies due to a high lattice oxygen mobility required to prevent coking in CH_4 dry reforming in realistic feeds.

This work aims at development of the mathematical description of catalytic gas-solid systems under unsteady conditions taking into account the lattice oxygen mobility and its application for the numerical investigation of transients of complex catalytic reaction. The quantitative estimation of the rates of lattice oxygen mobility and catalytic steps becomes

possible when the mathematical model of the system behavior reflects the processes in the gas phase, on the catalyst surface, and in the catalyst bulk.

Modeling studies with software developed are performed for two cases. To understand the impact of lattice oxygen mobility on the transient system behavior, firstly the theoretical analysis of the process dynamics is fulfilled for red-ox reaction with a model kinetic scheme. Then the response regimes for CH_4 dry reforming over Pt/CeZrPrO oxide catalyst are studied. The experimental data are analyzed by modeling, computational transient runs are performed to clarify the factors that control catalytic properties under unsteady conditions and evaluate the rates of bulk oxygen diffusion as well as main catalytic stages.

2. Mathematical description

The mathematical model was developed to describe dynamics of a catalytic reaction on the oxide catalyst in the flow reactor. The case under study is when one of the reagents in the gas mixture is oxidant, and the catalytic surface state along the length of the catalyst bed during kinetic transients is determined by the reaction proceeding on the active surface sites and the oxygen diffusion inside the near-surface layers of the catalyst.

The model is constructed on the following assumptions: (1) the effect of the gas diffusion along the z-axis of the catalyst bed and mass transfer from the gaseous flow to the catalyst surface is negligible, (2) diffusion in the catalyst pores influences insignificantly the reaction rates, (3) reaction proceeds on the surface of the nanoparticles of active component fixed as a porous layer on the corundum substrate, and (4) plug flow regime of the gas phase is realized in the reactor. It is supposed that the oxygen mobility in the catalyst bulk can be described by the diffusion mechanism with an effective coefficient D_V within subsurface layers.

Hence, the profiles of reagent concentrations in the gas phase along the reactor length with the axial coordinate l ($0 \le l \le L$, L is the length of the reactor) as well as the surface fractions of active species at each l position change with time t. The oxygen diffusion occurs in the catalyst

particle sublayer with coordinate h normal to the surface ($0 \le h \le H$, H is the maximum thickness of the near-surface layer of the catalyst particle involved in the oxygen exchange with the surface).

Mathematical description of the catalytic process in the isothermal reactor includes the following equations of mass balances with the corresponding initial (t = 0), inlet (l = 0), and boundary (h = 0 and h = H) conditions:

- for reaction mixture components in the gas phase (the equations of the kind "convection plus reaction on the catalyst surface" for unsteady-state conditions):

$$\varepsilon \frac{\partial c_i}{\partial t} = -\varepsilon u \frac{\partial c_i}{\partial l} - R_i, \quad i = 1, \mathrm{N} \tag{1}$$

$$l = 0: \quad c_i(t,0) = c_i^{in}, \qquad t = 0: \quad c_i(0,l) = c_i^0(l), \tag{2}$$

- for concentrations of oxidized sites or oxygen-containing species and active species (complexes, intermediates) on the catalyst surface which depend on the rates of catalytic stages and transport of oxygen species from the catalyst lattice:

$$\frac{\partial \theta_j}{\partial t} = r_j^{\theta}, \quad r_j^{\theta} = r_j^{\theta}(\theta_1(t,l),\ \theta_2(t,l),...,\theta_M(t,l),\ \theta_V(t,l,0)), \quad j = 1,\ldots,\mathrm{M}, \tag{3}$$

$$t = 0: \quad \theta_j(0,l) = \theta_j^0(l), \tag{4}$$

- for oxygen concentration in the catalyst lattice which is determined by the transport between the catalyst bulk and the surface:

$$\frac{\partial \theta_V}{\partial t} = D_V \frac{\partial^2 \theta_V}{\partial h^2}, \tag{5}$$

$$h = 0: \quad D_V \frac{\partial \theta_V}{\partial h} = \sigma r^V, \qquad h = H: \quad D_V \frac{\partial \theta_V}{\partial h} = 0, \tag{6}$$

$$t = 0: \quad \theta_V(0,l,h) = \theta_V^0(l,h). \tag{7}$$

Here in transport equations (1) and (2) $c_i(t,l)$ is the concentration of the *i*-th component (reagent or product) in the gas mixture, *N* is the number of the reactive components in the gas phase, ε is the fraction of the gas phase in the reactor volume, u is the velocity of the gas stream, R_i is the transformation rate of the *i*-th component of the gas mixture, c_i^{in} is the constant inlet concentration of the *i*-th component, and $c_i^0(l)$ determines the initial concentration profile of the *i*-th component along the reactor length.

For the equations (3) and (4) the symbols are as follows: $\theta_j(t,l)$ is the surface fraction of the *j*-th active species on the catalyst surface, M is the number of active surface species, r_j^{θ} is the formation rate of the *j*-th reactive species on the catalyst surface, and $\theta_j^0(l)$ stands for the initial concentrations of the *j*-th intermediate on the catalyst surface.

The designations in the equations (5)-(7) for oxygen concentration in the catalyst sublayer are as follows: $\theta_V(t,l,h)$ is the relative oxygen concentration in the catalyst bulk, D_V is the effective coefficient of oxygen diffusion in the near-surface layers of the catalyst particle, *H* is the characteristic thickness of near-surface catalyst bulk available for oxygen mobility, σ is the ratio of the fractions of the surface and subsurface oxygen, r^V is the transformation rate of θ_V species due to catalytic stages, and $\theta_V^0(l,h)$ denotes the initial concentration of oxygen in the catalyst lattice at each position along the axial coordinate of the reactor.

The resultant three-dimensional mathematical model (1)-(7) of unsteady processes in the isothermal reactor under study is the system that consists of the three groups of differential equations: the transport equations (1) for the concentrations of reagents and products $c_i(t,l)$ in the gas phase (with the coordinate *l* along the reactor length and time *t* as independent variables); the ordinary differential equations (3) for the surface fractions of oxidized sites and intermediates $\theta_j(t,l)$ (at each *l* position); and the parabolic partial differential equation (5) for the oxygen fraction in the near-surface catalyst layers $\theta_V(t,l,h)$ describing the lattice oxygen diffusion to the

surface active sites where the catalytic stages occur (with time *t* and coordinate *h* normal to the catalyst surface and directed into the catalyst particle bulk as independent variables; here the axial coordinate *l* is the variable which the boundary condition depends on). Hence, we have the initial-boundary-value problem for the system of (N + M + 1) differential equations of mixed type with three independent variables *t*, *h*, and *l* in the region

$$\Omega = \{(t,l,h): t \geq 0, 0 \leq l \leq L, 0 \leq h \leq H\}. \quad (8)$$

In the algorithm developed for solving the above problem we use the finite-difference approximation scheme of the second order with respect to two spatial coordinates *l* and *h* (axial coordinate along the reactor length and the distance from a point inside the oxide support particle to its surface) and time *t*. Method of the alternating directions is applied at each time step. The procedures allow to solve numerically the models of the kind (1)-(7) with different numbers N of reaction mixture components and M of surface species. Since the processes under study are rather complex and can have different characteristic time scales, the calculated distributions of concentrations in region Ω have large gradients. Therefore, the steps of discretization with respect to the time and space coordinates were chosen up to the values as small as $10^{-5} – 10^{-6}$ to ensure the approximation, stability, and accuracy of calculations [31].

3. Experimental

3.1. Catalyst characteristics

$Pr_{0.3}Ce_{0.35}Zr_{0.35}O_x$ mixed oxide was prepared via Pechini route, and Pt was supported by the incipient wetness impregnation as described in [14-29]. These samples were characterized by using XRD, TEM, neutronography, EXAFS, Raman, UV–Vis, O_2 TPD, FTIRS of adsorbed CO and oxygen isotope exchange, their reactivity was estimated by H_2 and CH_4 TPR, pulse reduction by CO and CH_4, reoxidation by pulses of O_2 and CO_2 [14-29].

To prepare a sample for studies of dynamic behavior of CH_4 dry reforming over Pt/PrCeZrO catalyst at short contact times in the flow reactor, a piece of a hollow thin-walled triangular

prismatic corundum substrate (wall thickness 0.2 mm, inner triangle side 2.33 mm, length 10 mm) was cut from an α-Al_2O_3 honeycomb monolith sintered at 1300 ^oC (specific surface area 3 m^2/g, porosity 0.4, average pore diameter 70 nm, pore volume 0.27 cm^3/g) [19-23]. A porous layer of complex PrCeZrO oxide prepared via Pechini route and calcined at 900 ^oC (specific surface area 30 m^2/g, measured by the express variant of the BET method using the data of argon thermal desorption in a SORBI-M instrument) was supported on this substrate by washcoating with the water suspension made by ultrasonically dispersing the oxide powder with the addition of polyvinyl butyral by several consecutive impregnations to provide loading of 7–10 wt% (layer thickness ca. 10 microns). After each impregnation, the samples were dried and calcined at 900 ^oC in air. Pt (1.6 wt%) was supported by the incipient wetness impregnation with H_2PtCl_6 solution followed by drying and calcination under air at 900 ^oC, which resulted in decrease of specific surface area of supported active component up to 20 m^2/g [16].

3.2. Transient studies

The transient data used for the computational analysis were obtained in the following way: the catalyst was pretreated in the oxygen stream at 700 ^oC, then reactor was purged by helium, and transients were recorded after switching the stream of He to that of the reaction mixture [16, 20]. The outlet concentrations of the reagents and reaction products were monitored by GC and online IR absorbance, electrochemical and polarographic sensors.

To provide high resolution kinetic transients, to minimize the dead time determined by the reactor purging when switching a stream of He to that of the reaction mixture, and to avoid thermodynamic limitations, short contact times (~ milliseconds) along with moderate concentrations of reagents (in the range of 5-10 vol.%) were shown to be required [16, 20-23, 27]. In turn, these requirements determine the operation temperature range in which conversions of reagents will be sufficiently high to follow reliably their variation in the kinetic transients, which is usually in the range of 600-800 ^oC, being rather close to that of the real structural catalysts operation in the natural gas dry reforming [32, 33]. Hence, experiments were carried

out under the following operation conditions: reaction gas flow consisting of methane, carbon dioxide, and helium was fed into the reactor with the gas flow rates of 5.6, 10.6, and 18 l/h, which correspond to the velocity of 70, 132, and 225 cm/s (STP). This variation of gas flow rates allowed to perform the experimental runs at different contact times of 15, 8, and 4.7 ms, respectively; both CH_4 and CO_2 inlet concentrations were equal to 7 vol.%. The reaction temperature was equal to 750 ^oC, the pressure was atmospheric.

4. Results and discussion

4.1. Catalysts characteristics

For $Pr_{0.3}Ce_{0.35}Zr_{0.35}O_x$ mixed oxide nanocrystalline structure formed of plate-like domains with typical sizes in the range of 10–15 nm (thickness ~ nm) was demonstrated by TEM, the most developed faces being of the (111) type. These domains are stacked into platelets with typical sizes up to 100 nm [14]. X-ray diffraction patterns correspond to single phase fluorite-like solid solution with the cubic structure. Neutron diffraction patterns are described by the tetragonal P42/nmc space group with c/a ratio close to 1, thus corresponding to so-called t''-phase [18, 26].

According to XPS and SIMS data [18], the surface is enriched by bigger Pr and Ce cations and is depleted by smaller Zr cations. This suggests that domain boundaries are as well enriched by bigger cations, thus explaining much higher rate of oxygen diffusion in the surface layer and along domain boundaries as compared with that in the bulk of domains estimated by using oxygen isotope transients [25].

For oxidized Pt/PrCeZrO sample Pt clusters and/or big particles were not revealed on the surface by TEM. XPS and FTIRS of adsorbed CO revealed domination of cationic Pt species demonstrating a strong Pt-support interaction [16, 18].

4.2. Kinetic studies

The consecutive studying various process components step-by-step is carried out with software developed considering three mathematical models of different level of complexity. At first, the theoretical analysis is performed with a model kinetic scheme to understand the impact of bulk oxygen mobility on the transients and estimate inherent time scales for oxygen bulk diffusion and catalytic reaction. Further the dynamic regimes for methane dry reforming are investigated. The experimental data and computational transient runs with simple and more complex kinetic schemes are analyzed to reveal features of the system behavior with catalyst oxygen mobility and estimate the coefficients of bulk diffusion with catalyst characteristics as well as kinetic parameters of the main catalytic stages.

4.2.1. Studies with a simplified kinetic scheme

The initial analysis of the reaction dynamics over catalysts with lattice oxygen mobility is performed using the simplest model kinetic scheme incorporated into the model of an isothermal plug flow reactor, the red-ox reaction is considered where oxygen is taken as oxidizing agent. The preliminary approach served to understand the main features of the system behavior, estimate the time scales of both process contributions, namely, catalytic surface reaction steps and oxygen supply via bulk mobility, as well as determine the range of oxygen diffusion rates in the near-surface layers of the catalyst structure, when the effect of the lattice oxygen mobility becomes significant.

The simplest model of the oxidation reaction is considered:

$$A + O_2 \rightarrow P.$$

It is assumed that the quantity of adsorption sites of reagent A on the catalyst surface is low and the rate of desorption stage of product P is higher significantly than the rates of other reaction stages. So, it is supposed that the surface state could be characterized by two types of centers – oxidized and vacant ones, and catalytic reaction occurs through two stages according to the red-ox mechanism via intermediate oxygen chemisorption on the vacant surface centers [Z] and transformation of reagent A on the oxidized centers [ZO]:

$$1.\ O_2 + 2\,[Z] \rightarrow 2\,[ZO]$$

$$2.\ A + [ZO] \rightarrow P + [Z] \qquad (9)$$

The reaction catalyzed by the oxide solid catalyst is studied along with the oxygen diffusion in the catalyst bulk and the main factors defining the oxygen surface coverage are the reaction stages (9) as well as the oxygen mobility in the oxide lattice.

Kinetic equations for the rates r_1 and r_2 of catalytic stages (9) were assumed to be defined on the basis of the mass action law and can be written as

$$r_1 = k_1 c_{O2} (1-\theta)^2, \qquad r_2 = k_2 c_A \theta, \qquad (10)$$

where c_A and c_{O2} are the concentrations of A and O_2 in the gas mixture, θ is the fraction of oxidized sites [ZO] on the surface, while k_1 and k_2 are the rate constants of the stages 1 and 2. Note, that here and below the relative dimensionless concentrations of reagents in the gas phase (i.e., volume fraction, $cm^3_{reagent}/cm^3_{mixture}$) are taken for modeling in the kinetic schemes.

The mathematical description (1)–(7) has been used for modeling with the reaction rates described by equations (10). The fraction of bulk oxygen θ_V in the boundary conditions (6) is assumed to be equal to the fraction of oxidized surface sites [11]. The reaction is considered after feeding the gas mixture containing the reagents A and O_2 to the reactor with inert gas in the empty volume (at time t = 0, there is no components A and O_2) and the catalyst with completely oxidized surface ($\theta^0(l) = 1$) till the achievement of the quasi-stationary characteristics of the system, i.e., the surface oxygen coverage and gas concentrations.

The transient regimes after feeding the reaction mixture on oxidized catalyst have been calculated and inherent time scales have been evaluated on the base of numerical experiments for both processes controlling the system properties – the chemical transformations and the lattice oxygen mobility. The reaction rates (constants k_1 and k_2), the reactor parameters (contact time τ = L/u), and the bulk oxygen diffusion rate (diffusion coefficient D_V) have been varied. The run

of modeled transient response data is exemplified in Fig. 1. There are given the curves of the effluent concentrations of reactants in the gas phase versus time (plots *a*, *b*, and *c*) and the fraction of oxygen surface coverage at the reactor outlet (plot *d*) with variation of the bulk oxygen diffusion rate.

It is seen that for low diffusion rate ($D_V = 10^{-19}$ cm^2/s, curves 1 in Fig. 1) the time range to attain the quasi-steady value for reagent A concentration c_A is short, less than 1 s (plot *a*), and further this concentration remains almost stationary during the following time period under study (plot *b*, curve 1); and the same effect is obtained for O_2 (plot *c*, curve 1). Similar time dependence is observed for the oxygen surface coverage: as the reagent concentration, the surface fraction of oxidized centers becomes equal to steady-state value in very short period (plot *d*, curve 1), and the lattice oxygen state remains invariable for all following time. For such value of diffusion rate the lattice oxygen mobility practically does not affect the surface state, and dynamics of the steady state achievement is controlled only by the reaction steps.

The effect of the lattice oxygen mobility becomes significant for some higher bulk diffusion rate, so in this case along with a fast transient for the reagent concentrations, subsequent slow transient to the steady-state gas composition is observed (Fig. 1). As for the case of a low diffusion rate, the time dependences are similar for both the reactant concentrations (plots *b* and *c*, curves 2 and 3) and the surface oxygen coverage (plot *d*, curves 2 and 3). This similarity for the gas components and the surface oxygen fraction indicates that the catalytic reaction stages in this longer time range are in the quasi-stationary state with respect to the gas mixture, the transient time scale of some hundred seconds is controlled by the rate of lattice oxygen diffusion and the bulk oxygen amount available for feeding the catalyst surface.

The short time of a jump of the reagent concentrations after feeding the reaction mixture on the oxidized catalyst is practically the same for all values of the bulk diffusion rates (plot *a*). This response time is determined by convection of the reacting gas mixture along the reactor and variation of the surface oxygen coverage due to the reaction stages. This response time is less

than 1 s for the example given in Fig. 1, and does not exceed a few seconds in all computational runs with other values of the reaction rates constants (k_1 and k_2 have been varied in the wide range of 1–50 s^{-1}) and contact time τ (0.03 – 1 s).

The slower changes of the system characteristics observed after jump of the gas composition (plots *b, c,* and *d* in Fig. 1) show that the subsequent gradual character of the response curves is caused by the lattice oxygen mobility. Under contact of the reaction mixture with the oxidized catalyst, formation of vacant centers on the surface occurs due to interaction of reagent A with the oxidized centers and generation of product P, while oxygen is supplied continuously from the near-surface layers and from the gas flow as well to the vacant centers keeping the oxidized surface state. For higher diffusion rate, the surface coverage by oxygen decreases slowly because of transport from the catalyst bulk (plot *d)*, that leads to a similar slow change of the reaction rate according to the catalytic stages (9) and to a similar character of the response curves of reagents (plots *b* and *c*, Fig.1).

The attempt has been made for the system under study to estimate the range of the bulk oxygen diffusion rates where, along with the first short interval of the response time, the other time scale related to the effect of the lattice oxygen mobility on the reaction rate is observed. It becomes apparent that, when the values of the diffusion coefficient D_V exceed 10^{-15} cm^2/s and are in the range of 10^{-14}–10^{-10} cm^2/s (curves 2 and 3 in Fig. 1), the achievement of the steady-state profiles of reactant concentrations occurs during the time interval exceeding 300 s. Hence, the difference in the time scales of the catalytic reaction and the bulk diffusion is about two orders of magnitude.

The results obtained in Section 4.2.1 allowed:

- to single out and estimate inherent time scales of the processes of different type - the catalytic reaction and the bulk oxygen diffusion,

- to determine the range of effective diffusion coefficients considering bulk oxygen mobility within the classic diffusion mechanism in a quasi-homogeneous system, where the effect of the lattice oxygen mobility is significant,
- to obtain the initial approximation of bulk diffusion rates for further studies with more complex kinetic schemes.

4.2.2. Studies of CH_4 dry reforming over Pt/CePrZrO catalyst

As was mentioned in Section 1, the impact of lattice oxygen mobility on the process performance was studied for nanocrystalline Pt-promoted ceria-zirconia catalysts doped with rare-earth elements (Gd, Pr, La) in several processes including dry reforming of methane. Pr-doped system was shown to provide the best activity in CH_4 dry reforming, which was explained by a high surface and bulk oxygen mobility required to suppress coking [16, 17, 19-23, 28, 29]. Some results of the kinetic transient analysis for a limited range of experimental parameters support this hypothesis [16]. More detailed analysis of this system behavior by modeling has been performed using the experimental data obtained for this catalyst in a broader range of operation conditions.

Figure 2 presents the results of transient experimental runs (outlet concentrations of reagents and products) carried out at different short contact times after feeding the reaction mixture on the oxidized catalyst and used for the analysis. The description of these experimental data can be found in [16] where the influence of subsurface/bulk oxygen mobility on the character of transients is reported. As it is seen, the main time interval where considerable change of the concentrations of reaction mixture components was observed is about 250–300 s. Analysis of the system with model reaction given in Section 4.2.1 shows also that such transient behavior can be caused by the effect of oxygen mobility in the catalyst bulk on its surface state.

The estimation of the resistance of the transport processes for applied structured design of the catalyst volume has been carried out. The Thiele criterion evaluated for the operation conditions under study with the values of catalyst activity in dry reforming given in [17] is lower than 0.1,

so the intra-particle diffusion in the catalyst pores does not influence the reaction rates significantly [16, 28, 34]. The rate of mass transfer between the gaseous flow and the external surface of the catalytic fragment wall is more than ten times higher in comparison with the reaction rate, and their impact can be neglected [28]. The impact of the axial diffusion at the studied conditions in this reactor system is slight as compared with the convective transport of the gas flow and could not be taken into consideration [16, 28, 35]. So, it can be supposed that the conditions of plug flow regime are realized in the reactor under study, and the mathematical model (1) – (7) described in Section 2 can be applied for the data processing to elucidate the intrinsic kinetic features.

Using the software developed, a number of computational transient runs have been performed to analyze and interpret the catalyst behavior, clarify the factors controlling catalytic properties and specific features of the reaction kinetics, and evaluate the rates of the catalytic stages. The process parameters used for modeling corresponded completely to the operation conditions of transient experiments given in Section 3. Two different kinetic schemes have been considered during modeling. At first a simplified 3-stage kinetic scheme was examined and then the simulation has been fulfilled with a more complex 6-stage reaction mechanism.

4.2.3. Modeling with 3-stage reaction scheme

According to the results of X-ray photoelectron spectroscopy and Fourier-Transform Infra-Red spectroscopy of adsorbed CO [16, 18], for oxidized Pt/PrCeZrO catalyst Pt is mainly in Pt^{2+} and Pt^{4+} states due to strong interaction with the support including incorporation of Pt cations into the surface cationic positions of doped ceria-zirconia. Since the concentration of cationic Pt forms increases with the Pr content in doped ceria-zirconia oxide, stabilization of Pt cations by Pr cations (or at least Pr cations along with Ce cations) can be suggested. Reduction of the oxidized Pt/PrCeZrO catalyst by CH_4 pulses revealed its high efficiency in CH_4 molecules activation by C-H bond rupture and oxidation of CH_x species into syngas, which can be assigned to a high reactivity of the $Pt^{n+}Pr^{3+/4+}O$ surface sites characterized by the heat of oxygen

adsorption ~ 200 kJ/mol [15, 16, 20, 24]. Note that this is a unique feature of oxidic Pt species stabilized by ceria-containing oxide supports since other metals (Ni, Ru, etc) are much less active in oxidic forms [36, 37]. Removal of oxygen by CH_4 pulses from Pt/PrCeZrO catalyst is accompanied by decline of the rate of reduction and increase of the heat of oxygen adsorption up to 650 kJ/mol corresponding to M_2O bridging species (M=Ce, Pr cations) [15, 24, 25]. Note that bridging surface oxygen species strongly bound with Zr cations (Zr_2O, CeZrO, etc) are considered to be non-reactive and not involved in diffusion processes. Hence, the most active oxidized $Pt^{n+}Pr^{3+/4+}O$ sites can be designated as [ZO] and reduced – as [Z]. Due to relatively low bonding strength of oxygen located on this specific center suggesting its coordination unsaturation (on-top or terminal oxygen form), this oxygen could interact with CO_2 molecules forming carbonate species [ZCO_3]. By analogy with known bifunctional schemes of CH_4 dry reforming including interaction of activated CH_x fragments adsorbed on the metal site with carbonate complexes adsorbed on oxide support sites [38], participation of [ZCO_3] complex in methane transformation into syngas can be considered as well.

In general, catalytic reaction stages can proceed on PtPrO centers as well as on the sites of the PrCeZrO oxide support. A high initial rate of CH_4 reforming on the oxidized surface as well as its continuous decline with time due to progressive reduction of [ZO] centers by the reaction feed agree with the results of pulse studies [15, 24, 25]. Bulk and surface oxygen mobility of complex oxide support counteracts this decline of activity by supplying oxygen atoms to reduced [Z] centers. The surface oxygen species of support, on the one hand, are consumed via transfer to [Z] sites (where they interact with CH_4) and, on the other hand, are regenerated due to CO_2 dissociation on reduced support sites as well as by oxygen diffusion from the subsurface/bulk oxide layers.

A simple reaction mechanism could be considered for system modeling to analyze the main features of the catalyst behavior and estimate the rates of main stages: methane is oxidized on the active [ZO] centers which are regenerated due to oxygen species migration from the surface sites

as well as from the near-surface layers of complex oxide support. Dissociation of carbon dioxide on the surface oxygen vacancies of support generating mobile bridging oxygen forms also provides required replenishment of the reactive oxygen species.

The kinetic scheme consisting of three stages is used:

- CH_4 transformation occurs on the oxidized sites [ZO],
- vacant centers [Z] are reoxidized by the surface oxygen [O_S] supplied from the surface sites as well as from the subsurface layers of support,
- CO_2 interacts with the surface oxygen vacancies [V_S] of the support with formation of carbon monoxide:

$$\begin{aligned} &1.\ CH_4 + [ZO] \rightarrow 2\,H_2 + CO + [Z], \\ &2.\ [O_s] + [Z] \leftrightarrow [ZO] + [V_s], \\ &3.\ CO_2 + [V_s] \rightarrow CO + [O_s]. \end{aligned} \qquad (11)$$

Here [ZO] and [Z] are oxidized and reduced Pt-containing active centers on the catalyst surface, while [O_s] and [V_s] are the oxidized and reduced sites of the oxide support determined by the surface concentration of Ce and Pr cations (vide supra). The corresponding stoichiometric pathway is

$$CH_4 + CO_2 \leftrightarrow 2\,H_2 + 2\,CO. \qquad (12)$$

The rates of all other possible reactions are assumed to be negligible.

The rates of catalytic stages (11) are supposed to satisfy the mass action law as follows:

$$r_1 = k_1 c_{CH4}\,\theta_1, \quad r_2 = k_2\,\theta_2(1-\theta_1), \quad r_{-2} = k_{-2}\,\theta_1(1-\theta_2), \quad r_3 = k_3 c_{CO2}\,(1-\theta_2). \qquad (13)$$

Here r_i is the rate of the i-th catalytic stage (i = 1, 2, -2, 3); c_{CH4} and c_{CO2} are concentrations of CH_4 and CO_2 in the gas mixture, respectively; θ_1 is [ZO] fraction on the surface; θ_2 is the relative surface concentration of oxidized centers [O_s] of the support; and k_i is the rate constant of the i-th stage (i = 1, 2, -2, 3).

For defining the fractions of surface sites, their total quantity on the catalyst surface has been assumed as approximate to the number of monolayer surface coverage with oxygen atoms $N_\theta = 1.28 \cdot 10^{15}$ atoms O/cm^2 including inert oxygen species strongly bound with Zr cations. The maximal fraction of [ZO] centers has been denoted by α, and that of [O_s] sites, by β, where $\alpha + \beta < 1$. Then θ_1 is equal to the ratio of the number of [ZO] surface centers N_{ZO} to their maximal number αN_θ, and θ_2 is the ratio of the number of [O_s] sites N_{OS} to their maximal number βN_θ:

$$N_{ZO} + N_Z = \alpha N_\theta, \quad \theta_1 = N_{ZO}/\alpha N_\theta, \quad N_{OS} + N_{VS} = \beta N_\theta, \quad \theta_2 = N_{OS}/\beta N_\theta, \qquad (14)$$

where N_Z and N_{Vs} stand for the numbers of reduced centers on the catalyst surface [Z] and reduced sites of the oxide support [V_s], respectively. The fraction of [Z] centers is equal to ($1 - \theta_1$), and the fraction of [V_s] sites is ($1 - \theta_2$).

Reverse water-gas-shift reaction was not considered for this simple scheme since its impact should only increase CO_2 consumption with the catalysts reduction by the reaction feed in contrary to observed trend (vide infra).

Computational studies have been carried out with the mathematical description (1)–(7) presented in Section 2, where the indices i correspond to methane (i = 1), carbon dioxide (i = 2), carbon monoxide (i = 3), and hydrogen (i = 4); the indices j =1,2 are used for the equations (3) with the surface fractions θ_1 and θ_2; and the rates of the reagent transformations and alteration of the surface coverage correspond to the formulas (11) and (13). It is assumed that, after catalyst pretreatment in the oxygen flow before reaction mixture feeding, the vacant centers [Z] and [V_s] are absent; i.e., $\theta_1^0(l) \equiv 1$ and $\theta_2^0(l) \equiv 1$ for t = 0 (see the initial conditions (4) in the model). For the equation (5) the initial conditions (7) on the surface were taken as $\theta_V^0(l,h) = \theta_2$. All operation parameters correspond to those for experiments.

The initial approximation for the parameters in the model (1) – (7) was derived by the following way. The initial values for the rate constants are supposed from analysis of the data on the steady state catalyst activity [17]. The catalyst structural parameters (namely, the maximal fractions of the surface occupied by active oxidized centers and the support surface covered by reactive oxygen species as well as the characteristic depth of the near-surface layers involved in fast oxygen migration) were based upon their characterization by physical methods TEM, XPS, FTIRS, etc [15, 16, 18]. The range of the oxygen diffusion coefficient variation has been chosen as 10^{-14} – 10^{-10} cm^2/s, this interval corresponds to the calculated response times about 300 s for the model kinetic scheme (Section 4.2.1, Fig. 1) and agrees with the results of D_V estimation by oxygen isotope heteroexchange [25, 26, 39] and chemical transients [27].

Figures 3 and 4 give some numerical results and show the calculated transient regimes for CH_4 and CO_2 concentrations and dynamics of the bulk and surface oxygen fractions (all curves correspond to the reactor outlet, $l = L$). Influences of the diffusion coefficient and the capacity of the subsurface catalyst layer involved in oxygen migration are shown in Fig. 3. For all operation conditions a monotonous increase of CH_4 concentration is seen, while CO_2 concentration decreases with time. According to the kinetic scheme (11), at the beginning the methane transformation occurs rapidly on the oxidized centers (stage 1), then its rate decreases with the catalyst surface reduction by the reaction mixture, while the bulk oxygen diffusion counteracts this reduction (stage 2). On the contrary, at first CO_2 consumption rate is low since the largest part of the support surface sites is in the oxidized state as well (stage 3 is very slow). The transient time of CH_4 and CO_2 concentrations (Fig. 3) as well as bulk and surface oxygen fractions (Fig. 4) is about 300 s. Hence, these transients are determined by oxygen diffusion from the near-surface layers of the catalyst support to the surface. Note that in each plot the asymptotic values of concentrations of CH_4, CO_2 and θ_V coincide since they are independent of the oxygen bulk diffusion rate.

Compare the curves 1 and 2 in Fig. 3. The bulk oxygen diffusion is more intensive in case 2. At first moment of the catalyst contact with the reaction feed and for up to about 80 s, methane is being consumed faster in case 2 because the active sites on the surface have been oxidized faster and stage 1 occurs there. At the same time, CO_2 reacts more slowly in case 2 since, due to the bulk oxygen transport to the surface, we have faster recuperation of [ZO] at the surface than appearance of [V_s] sites required for stage 3. For t > 80 s the influence of the bulk oxygen diffusion on the rates of CH_4 and CO_2 consumption becomes less. The curves 2 and 3 correspond to the same diffusion coefficient D_V but different capacity of the near-surface bulk lattice with respect to oxygen. Therefore, in case 3 the surface sites are oxidized faster than in case 2 and the rate of stage 1 is higher, while the rate of stage 3 is lower; and, hence, CO_2 concentration in the effluent gaseous mixture is higher, while CH_4 concentration is lower.

The supposition on rather high efficiency of the oxidized surface species in methane activation is confirmed by a qualitative agreement between the calculated line and the experimental points of transients for CH_4 concentration (Fig. 5). Lower experimental values of methane concentration as compared with the numerical curve indicate that some additional stage of methane transformation can occur. On the other hand, modeling and experimental CO_2 curves differ drastically: the opposite transient behavior of the concentrations of CH_4 and CO_2 has been obtained in the modeling runs, while a similar character of their transients is seen in the experiments. Since the experimental CH_4 and CO_2 transients are parallel, more efficient CO_2 transformation on the oxidized surface sites should be suggested as well. Basing on these results, we can conclude that the additional stages of CH_4 and CO_2 conversion occurring on the oxidized surface centers should be included in the kinetic system for further analysis.

Experimental data processing has shown also that the calculated time of the system stabilization corresponds to experimental one if the diffusion coefficient D_V lies in the range of $10^{-13} – 10^{-12}$ cm^2/s. It agrees with the response data observed for the simplified kinetic scheme in Section 4.2.1 (vide supra). The numerical data with 3-stage kinetic scheme show that as for the

model kinetic scheme, transient time scale of some hundred seconds is determined by the rate of the internal bulk transport of oxygen species.

Hence, the results of system modeling with 3-stage kinetic scheme and experimental data processing allowed:

- to show that longer time scale observed in the experimental transients is controlled by the internal transport of oxygen species and to evaluate the range of diffusion coefficient D_V;
- to determine that, as for model kinetic scheme, the surface coverages are largely affected by oxygen transport from the bulk;
- to estimate the CH_4 conversion rate and to show which additional reaction stages should be included into the reaction scheme under consideration;
- to derive the data for initial approximation of parameters needed for the further data processing.

4.2.4. Modeling with 6-stage reaction scheme

On the base of literature data [38, 39] as well as the results obtained by modeling in Section 4.2.3 the kinetic reaction scheme has been modified as follows: the steps of formation of the carbonate complexes and their interaction with CH_4 have been included and, in addition, analysis of the data obtained with the 3-stage kinetic scheme shows that the reverse water-gas-shift reaction (RWGS) route should be considered too [27].

Existence of a variety of carbonates on the surface of catalysts based on doped ceria-zirconia oxides with supported metals under contact with CO_2 was shown in our research [25]. Bridging carbonates retained on the steady-state surface of catalyst after removing the reaction feed are not very reactive with respect to CH_4, but it does not exclude a high reactivity of less strongly bound terminal carbonates adsorbed on the surface support in vicinity of Pt^{2+} cations for the initial oxidized catalyst with supported Pt.

The modified reaction scheme consists of six steps and the following three stages have been added to the kinetic scheme (11):

- CO_2 interaction with the oxidized sites [ZO] yielding carbonates [ZCO_3],
- participation of [ZCO_3] complex in CH_4 transformation,
- H_2 interaction with the oxidized surface sites [ZO] as a stage required for providing RWGS reaction route.

The subsequent modeling studies have been carried out on the base of the 6-stage kinetic scheme given in Table 1, where the notations are similar (see below) to the symbols for 3-stage scheme. Here [ZO] and [Z] are oxidized and reduced Pt-containing surface centers, [O_s] and [V_s] correspond to the oxidized and reduced sites of the oxide support, and [ZCO_3] are carbonate complexes on the surface.

This scheme includes two routes for CH_4 dry reforming through interaction with carbonate complexes (route I) as well as with oxidized active sites (route II), while route III provides reverse water-gas-shift reaction. As for the 3-stage scheme, it has been supposed that the rates of the Boudouard reaction and methane decomposition are negligible in the time range under study; so the coke formation does not occur due to the oxygen supply from the catalyst bulk to the surface [15, 16].

The rate equations of reaction stages have been supposed to conform to the mass action law as for the 3-stage scheme and look as follows:

$$r_1 = k_1 c_{CO2} \theta_1, \quad r_{-1} = k_{-1} \theta_3, \quad r_2 = k_2 c_{CH4} \theta_3, \quad r_3 = k_3 c_{CH4} \theta_1, \tag{15}$$

$$r_4 = k_4 (1 - \theta_1 - \theta_3) \theta_2, \quad r_{-4} = k_{-4} \theta_1 (1 - \theta_2), \quad r_5 = k_5 c_{CO2} (1 - \theta_2), \quad r_6 = k_6 c_{H2} \theta_1.$$

Here, like in the equations (13), r_i is the rate of the i-th catalytic stage (i = 1, 2, …, 6); c_{CH4}, c_{CO2}, and c_{H2} are the concentrations of CH_4, CO_2, and H_2 in the gaseous reaction mixture, respectively; k_i is the rate constant of the i-th stage (i = 1, 2, …, 6); θ_1 is [ZO] fraction on the surface; θ_2 is the relative surface concentration of oxidized centers [O_s] of the support; and θ_3 is the relative concentration of carbonate complexes [ZCO_3] on the surface. The expressions for the

relative concentration of the active centers correspond to the equations (14), only adding in this case

$$N_{ZO} + N_{ZCO3} + N_Z = \alpha N_\theta , \quad \theta_3 = N_{ZCO3}/\alpha N_\theta , \tag{16}$$

where N_{ZCO3} stands for the number of carbonate complexes [ZCO_3] on the surface,

Numerical transient studies have been performed also on the base of mathematical model (1)–(7) used for the runs with the 3-stage kinetic scheme (11). The following modifications have been made: the equation for θ_3 has been added and the kinetic equations (15) have been applied, so the system (1) was considered for concentrations of CH_4, CO_2, CO, and H_2 in the gas flow. Modeling runs have been implemented to analyze the broader set of experimental response data (Fig. 2) performed at the contact time of 4.7, 8, and 15 ms. Numerical solutions were found taking the reactor parameters and operation conditions corresponding completely to those for transient experiments.

The initial values of the parameters were estimated as follows. The constants of the reaction steps have been evaluated combining the initial approximation for the 3-stage kinetic scheme obtained from the catalyst activity data at stationary state [17] and some kinetic parameters derived from the results of processing with this scheme (see Section 4.2.3). The catalyst structural and surface parameters were estimated on the base of catalyst characterization by physical methods (TEM, XPS, FTIRS, etc [15, 16, 18]) and processing results with 3-stage scheme as well (see Section 4.2.3). The initial state of the catalyst surface is assumed to be oxidized completely (i.e., $\theta_1^0 = \theta_2^0 = 1$). The time scale in the range of 300 s was also considered, for which significant gradients of the concentration were observed in the experimental transients. The interval of 10^{-13} – 10^{-12} cm^2/s for diffusion coefficients D_V was estimated during processing with the 3-stage kinetics (Figs. 3–4).

Figures 6–9 present the modeling results of the system behavior with variation of the oxygen diffusion rate; the calculated relative concentrations of the active centers on the catalyst surface and the bulk oxygen fraction as well as dynamics of the reagent and product concentrations in

the gas phase are given. All curves correspond to the points at the reactor outlet ($l = L$).

Figure 6 shows modeling values of the surface center fractions occupied by oxygen [ZO] and carbonates [ZCO_3]. In the frame of 6-stage kinetic scheme, at first, after switching to the reaction mixture, methane and carbon dioxide are consumed with high rates (stages 1, 2, and 3). Such catalyst activity is provided by the oxidative pretreatment due to enhanced activity of the oxidized sites [ZO]. Hence, reduction of these sites and, respectively, the surface oxygen centers [O_S] of the oxide support occurs. At the same time, bulk oxygen mobility of Pr-doped catalyst counteracts the reduction by supplying oxygen atoms to the reduced centers of the support at the surface, and the reduced active sites [Z] are oxidized by the surface oxygen coming from the near-surface layers of the support. The higher the bulk diffusion rate becomes, the slower is the reduction of the surface in the time period ~ 50 s. Further, the fraction of the oxidized active sites [ZO] decreases slowly and stabilizes in the time range of about 300 s. The surface coverage by carbonates [ZCO_3] attains the maximal value very quickly after switching to the reaction feed (stage 1), then it declines with time due to interaction with CH_4 (stage 2) leading to [ZO] centers reduction while CO_2 oxidizes the reduced [V_s] sites too (stage 5).

The dependence of oxygen distribution in the catalyst bulk on the diffusion rate is shown in Fig. 7. After reagent mixture supply, the oxygen content in the near-surface layers of the support lattice declines rather sharply, the vacant centers [Z] are rapidly formed on the catalyst surface due to high rates of the catalyst interaction with methane (stage 3), and their stabilization is affected by the oxygen diffusion from the near-surface layers of support. The decrease of the diffusion rate leads to a broader and longer variation of the oxygen distribution along the depth of the support lattice. The slower is the lattice oxygen diffusion, the weaker is the oxygen supply from the near-surface oxide layers to the surface, thus increasing the transient time interval for achieving the quasi-steady state of the system.

Modeling data on the dynamics of the gas composition corresponding to the examples of transient catalyst characteristics (Figs. 6 and 7) are given in Figs. 8 and 9. In a short initial time

interval after switching to the reaction feed, a rapid (in a few seconds) change of CH_4 and CO_2 concentrations as well as CO and H_2 products are observed. This time scale is determined only by the rates of reaction stages, so it is very short due to high Pt/PrCeZrO catalyst activity in this process realized at millisecond contact times. Subsequent time scale is about 300 s, when some significant change of the reagent concentrations occurs, the period of these transients being completely determined by variation of the catalyst bulk oxygen content. For the products, the transient behavior is the same as for reagents (see Fig. 9).

Comparison of the gas phase and catalyst response characteristics at different oxygen diffusion rates shows that transients of the gas-phase components (i.e., the reaction rates in this time period) are determined by a slow accumulation of the reduced centers on the surface due to interaction with the reaction mixture; this process being counteracted by the oxygen supply from the bulk lattice layers to the surface. As for the oxygen distribution in the catalyst bulk, decrease of the lattice oxygen mobility leads to longer variation of the reagent and product concentrations, the time interval for attaining the quasi-stationary conditions increases.

The comparison of modeling results obtained with three kinetic schemes shows that for different sets of catalytic stages the transient time scale defined by the chemical transformations on the surface does not exceed a few seconds. A considerable change of the reaction rates observed for the time about 300 seconds is due to variation of the catalyst surface coverage by oxygen which is determined by diffusion of the oxygen species from the bulk of oxide support. For the kinetic schemes considered, this response period is practically the same at equal values of the rates of bulk oxygen diffusion and the structure parameters. So, the analysis of the data for three variants of kinetic schemes performed in the broad range of operating conditions confirms the summary of [16] reliably that: (1) time scales determined by reaction stages occurrence are not higher than some seconds, and (2) time scales due to bulk oxygen diffusion belong to the range of several hundred seconds.

In contrast to the 3-stage scheme, the suggested 6-stage kinetic scheme reflects main features of the transient behavior of this system. Figures 8 and 9 show that the character of the modeled response curves for CH_4 and CO_2 concentrations is similar and corresponds to the transients observed in the experiments (Fig. 2) due to carbonate formation on [ZO] centers. The experimental and numerical transient data for H_2 and CO products have similar character as well. Hence, it can be concluded on the base of these data and studies with modeled and 3-stage kinetic schemes provided in Sections 4.2.1 and 4.2.3 that the specific features of the reaction kinetic scheme define the type and form of the transient curves, while the slow response time interval does not depend on the set of reaction stages and their rates.

Processing the whole set of experimental data obtained at contact times of 4.7, 8, and 15 ms has been performed with 6-stage kinetic scheme, and the range of parameters has been derived when a satisfactory description of experimental transients is attained, which looks as follows:

- the catalyst characteristics:

  - the maximal fractions of the surface occupied by active oxidized centers and the support surface covered by reactive oxygen species

    $\alpha = 0.04 \div 0.05$ and $\beta = 0.2 \div 0.25$, respectively,

  - the coefficient and the characteristic length of bulk oxygen diffusion

    $D_V = 2 \cdot 10^{-13} \div 3 \cdot 10^{-13}$ $cm^2 s^{-1}$ and $H = 3 \cdot 10^{-6} \div 4 \cdot 10^{-6}$ cm, respectively;

- the constants of reaction stage rates:

$$k_1 = 170 \div 230\ s^{-1}, \quad k_{-1} = 0.5 \div 1\ s^{-1}, \quad k_2 = 450 \div 600\ s^{-1}, \quad k_3 = 50 \div 70\ s^{-1},$$

$$k_4 = 250 \div 300\ s^{-1}, \quad k_{-4} = 5 \div 10\ s^{-1}, \quad k_5 = 40 \div 55\ s^{-1}, \quad k_6 = 400 \div 1100\ s^{-1}.$$

Since thus estimated characteristic length of bulk oxygen diffusion is close to the average radius of fluorite-like support particles (~ $3 \cdot 10^{-6}$ cm) [16], this means that at 750 ^oC oxygen migration affects all bulk of oxide support particles. The values of the support coverage by reactive oxygen species agree with the amount of oxygen removed at 700 ^oC by a pulse of 7%CH_4 in He from the surface of this catalyst in the steady state of CH_4 dry reforming [24] as

well as by pulses of 1% CO in He at 500 ^{o}C from the surface of oxidized doped ceria-zirconia support~30% of monolayer [43]. Estimation of α corresponding to the surface fraction occupied by Pt cations reasonably agrees with XPS data for the doped ceria-zirconia samples prepared by the same procedures with close values of Pt loading giving atomic ratio of Pt surface concentration to the sum of all cations ~ 0.04 [27].

As shown in Figs. 10 and 11, a rather good agreement between the experimental and modeled transients for reagents and products is seen. Hence, the experimental data (especially parallel CO_2 and CH_4 transients) have been described in frames of the 6-stage scheme with a due regard for the specificity of the reaction mechanism and the lattice oxygen mobility. Though importance of the oxygen species diffusion from the fluorite-like oxide support to the metal-support interface for providing coking stability of Me-supported catalysts in methane dry reforming was proposed in many studies [13, 14, 40-42], however, direct estimation of the respective rate constants was absent up to studies reported in [16, 25, 27] and this work. Apparently the best agreement between experimental and modeling transients of CH_4 and CO_2 was achieved for experiments carried out at the shortest contact time of 4.7 ms, i.e., in conditions where the gradient of reagents concentrations along the channel length is minimal. Since this model does not take into account enhanced oxygen mobility along nanodomain interfaces in doped ceria-zirconia support as well as effect of its stoichiometry on the oxygen diffusion characteristics [25, 27], it implies that more detailed analysis should also take into account variation of D_V along the channel length.

The data presented here confirm the preliminary results about the mechanism of methane dry reforming on Pt/PrCeZrO stated in [16] where unique ability of oxidized sites comprised of Pt and Pr cations in activation of both reagents was revealed. The numerical experiments with modeled kinetic scheme show the influence of lattice oxygen mobility on the behavior of similar catalytic system, time scales controlling different transient periods have been clarified, and the range of oxygen diffusion rates have been estimated. The studies of dry reforming mechanism

with 3-stage kinetic scheme allow the following: (1) to estimate the rate of the CH_4 transformation, (2) obtain the valuable information about additional reaction stages, and (3) derive additional data for initial parameters approximation during further processing with 6-stage reaction scheme. This processing performed with the broader data set of experimental data and the independent estimations of some parameters decreases uncertainty in determination of system characteristics, confirms the hypothesis about suggested dry reforming mechanism [16], and increases significantly its reliability.

5. Conclusion

The complex catalytic reaction occurring under unsteady conditions is appropriately described using a mathematical model and implementation of the software developed in this work. Processes accounted by the model include convective gas transport, reactions on the catalyst surface and diffusion of oxygen-containing species from the subsurface of support to the surface. A red-ox reaction model describes the dynamics of the catalytic surface reaction in the flow reactor. Oxygen mobility in subsurface layers of the support is considered with the classic diffusion mechanism in a quasi-homogeneous system. Since this model does not take into account enhanced oxygen mobility along nanodomain interfaces in doped ceria-zirconia support, it could explain incomplete match of experimental transient data and their model fitting for some experimental conditions. The experimental transient data on CH_4 dry reforming over Pr-doped ceria-zirconia oxide supported Pt catalyst (Pt/CeZrPrO) gave a suitable match to parameter optimized predictions of an applicable model. Model and parameter comparison clarified the factors controlling catalytic properties and catalytic reaction rates.

Modeling results on three kinetic schemes show that the time scale to approach a quasi-steady state of the catalyst that is defined by chemical transformations on the surface does not exceed a few seconds under considered conditions. Substantial change in the reaction rates observed over a time scale of several hundred seconds is caused by variation of the catalyst surface coverage related to the oxygen species diffusion from the bulk of the oxide support.

Characteristics of the transient data traces are sensitive to the involved kinetic scheme thereby providing hints on the reaction mechanism. High efficiency of cationic Pt species in CH_4 dissociation is confirmed, and it is shown that CO_2 transformation may occur via formation of carbonates. Kinetic parameters of the catalytic surface reactions and the rate of bulk oxygen diffusion were estimated in parallel to characteristics of the catalyst surface state and oxygen non-stoichiometry in the surface/bulk layers. In summary, the presented exploitation of transient kinetic data complements the catalyst characterization by physical methods to extract reliable information about the state of the catalyst surface/subsurface and the reaction mechanism.

Acknowledgements

This work was conducted within the framework of budget projects No. 0303-2016-0013 and No. 0303-2016-0017 for Boreskov Institute of Catalysis. Support by the European Commission in the 7th Framework Programmes OCMOL (GA 228953) and BIOGO (GA 604296), Ministry of the High Education and Science of the Russian Federation, and SB RAS Interdisciplinary Integration Project no. 80 is gratefully acknowledged.

References

[1] R.J. Berger, F. Kapteijn, J.A. Moulijn, G.B. Marin, J.D. Wilde, M. Olea, D. Chen, A. Holmen, L. Lietti, E. Tronconi, Y. Schuurman, Dynamic methods for catalytic kinetics, Applied Catalysis A: General 342 (2008) 3–28.

[2] A.M. O'Connor, Y. Schuurman, J.R.H. Ross, C. Mirodatos, Transient studies of carbon dioxide reforming of methane over Pt/ZrO_2 and Pt/Al_2O_3, Catalysis Today 115 (2006) 191–198.

[3] Y. Schuurman, Assessment of kinetic modeling procedures of TAP experiments, Catalysis Today 121 (2007) 187–196.

[4] V. Balcaen, R. Roelant, H. Poelman, D. Poelman, G.B. Marin, TAP study on the active oxygen species in the total oxidation of propane over a $CuO\text{-}CeO_2/\gamma\text{-}Al_2O_3$ catalyst, Catalysis Today 157 (2010) 49–54.

[5] R. Roelant, D. Constales, R.V. Keer, G.B. Marin, Identifiability of rate coefficients in linear reaction networks from isothermal transient-experimental data, Chem. Eng. Sci. 65 (2010) 2333–2343.

[6] I. Nowa, L. Letti, E. Tronconi, P. Forzatti, Transient response method applied to the kinetic analysis of the $DeNO_x$–SCR reaction, Chem. Eng. Sci. 56 (2006) 1229–1237.

[7] M. Colombo, I. Nova, E. Tronconi, Detailed kinetic modeling of the NH_3–NO/NO_2 SCR reactions over a commercial Cu-zeolite catalyst for Diesel exhausts after treatment, Catalysis Today 197 (2012) 243–255.

[8] M. García-Diéguez, I.S. Pieta, M.C. Herrera, M.A. Larrubia, I. Malpartida, L.J. Alemany, Transient study of the dry reforming of methane over Pt supported on different $\gamma\text{-}Al_2O_3$, Catalysis Today 149 (2010) 380–387.

[9] J. Guo, H. Lou, L. Mo, X. Zheng, The reactivity of surface active carbonaceous species with CO_2 and its role on hydrocarbon conversion reactions, J. Molec. Catal. A: Chemical 316 (2010) 1–7.

[10] V.D. Sokolovskii, Principles of oxidative catalysis on solid oxides, Catal. Rev. - Sci. Eng. 32 (1990) 1–49.

[11] N.M. Ostrovskii, S.I. Reshetnikov, The influence of oxygen mobility in solid catalyst on transient regimes of catalytic reaction, Chem. Eng. J. 107 (2005) 141–146.

[12] M. Salazar, D.A. Berry, T.H. Gardner, D. Shekhawat, D. Floyd, Catalytic partial oxidation of methane over Pt/ceria-doped catalysts: Effect of ionic conductivity, Applied Catalysis A: General 310 (2006) 54–60.

[13] D.K. Kim, K. Stöwe, F. Müller, W.F. Maier, Mechanistic study of the unusual catalytic properties of a new Ni–Ce mixed oxide for the CO_2 reforming of methane, J. Catal. 247 (2007) 101–111.

[14] V. Sadykov, V. Muzykantov, A. Bobin, N. Mezentseva, G. Alikina, N. Sazonova, E. Sadovskaya, L. Gubanova, A. Lukashevich, C. Mirodatos, Oxygen mobility of Pt-promoted doped CeO_2–ZrO_2 solid solutions: Characterization and effect on catalytic performance in syngas generation by fuels oxidation/reforming, Catalysis Today 157 (2010) 55–60.

[15] V.A. Sadykov, N.N. Sazonova, A.S. Bobin, V.S. Muzykantov, E.L. Gubanova, G.M. Alikina, A.I. Lukashevich, V.A. Rogov, E.N. Ermakova, E.M. Sadovskaya, N.V. Mezentseva, E.G. Zevak, S.A. Veniaminov, M. Muhler, C. Mirodatos, Y. Schuurman, A.C. van Veen, Partial oxidation of methane on Pt-supported lanthanide doped ceria-zirconia oxides: Effect of the surface/lattice oxygen mobility on catalytic performance, Catalysis Today 169 (2011) 125–137.

[16] V.A. Sadykov, E.L. Gubanova, N.N. Sazonova, S.A. Pokrovskaya, N.A. Chumakova, N.V. Mezentseva, A.S. Bobin, R.V. Gulyaev, A.V. Ishchenko, T.A. Krieger, C. Mirodatos, Dry reforming of methane over Pt/PrCeZrO catalyst: Kinetic and mechanistic features by transient studies and their modeling, Catalysis Today 171 (2011) 140–149.

[17] N.N. Sazonova, V.A. Sadykov, A.S. Bobin, S.A. Pokrovskaya, E.L. Gubanova, C. Mirodatos, Dry reforming of methane over fluorite-like mixed oxides promoted by Pt, React. Kinet. Catal. Lett. 98 (2009) 35–41.

[18] V.A. Sadykov, N.V. Mezentseva, G.M. Alikina, A.I. Lukashevich, Yu.V. Borchert, T.G. Kuznetsova, V.P. Ivanov, S.N. Trukhan, E.A. Paukshtis, V.S. Muzykantov, V.L. Kuznetsov, V.A. Rogov, J. Ross, E. Kemnitz, C. Mirodatos, Pt-supported nanocrystalline ceria-zirconia doped with La, Pr or Gd: factors controlling syngas generation in partial oxidation/autothermal reforming of methane or oxygenates, Solid State Phenomena 128 (2007) 239–248.

[19] S. Pavlova, N. Sazonova, V. Sadykov, S. Pokrovskaya, V. Kuzmin, G. Alikina, A. Lukashevich, E. Gubanova, Partial Oxidation of Methane to Synthesis Gas over Corundum Supported Mixed Oxides: One Channel Studies. Catal. Today 105 (2005) 367–371.

[20] E.L. Gubanova, A.C. van Veen, C. Mirodatos, V.A. Sadykov, N.N. Sazonova, Influence of the Mobility of Oxygen in a Complex Oxide Carrier on the Mechanism of Partial Oxidation of Methane, Russian Journal of General Chemistry 78 (2008) 2191–2202.

[21] N.N. Sazonova, V.A. Sadykov, A.S. Bobin, S.A. Pokrovskaya, E.L. Gubanova, C. Mirodatos, Partial oxidation of methane into synthesis gas over a Pt-supported complex fluorite-like oxide: one-channel studies in realistic feeds, React. Kinet. Catal. Lett. 98 (2009) 19–26.

[22] N.N. Sazonova, V.A. Sadykov, A.S. Bobin, S.A. Pokrovskaya, E.L. Gubanova, C. Mirodatos, Partial oxidation of methane into syngas on Pt-supported mixed oxides: effect of surface/lattice oxygen mobility in complex oxides on the kinetic features of the reaction and performance stability, React. Kinet. Catal. Lett. 98 (2009) 27–33.

[23] E.L. Gubanova, Y. Schuurman, V.A. Sadykov, C. Mirodatos, A.C. van Veen, Evaluation of kinetic models for the partial oxidation of methane to synthesis gas over a Pt/PrCeZrOx catalyst coated on a triangular monolith, Chem. Eng. J. 154 (2009) 174-178.

[24] V. Sadykov, V. Rogov, E. Ermakova, D. Arendarsky, N. Mezentseva, G. Alikina, N. Sazonova, A. Bobin, S. Pavlova, Y. Schuurman, C. Mirodatos, Mechanism of CH_4 dry reforming by pulse microcalorimetry: Metal nanoparticles on perovskite/fluorite supports with high oxygen mobility, Thermochimica Acta 567 (2013) 27–34.

[25] A.S. Bobin, V.A. Sadykov, V.A. Rogov, N.V. Mezentseva, G.M. Alikina, E.M. Sadovskaya, T.S. Glazneva, N.N. Sazonova, M.Yu. Smirnova, S.A. Veniaminov, C. Mirodatos, V. Galvita, G.B. Marin, Mechanism of CH_4 dry reforming on nanocrystalline doped ceria-zirconia with supported Pt, Ru, Ni, and Ni–Ru, Topics in Catalysis 56 (2013) 958–968.

[26] Vladislav Sadykov, Natalia Mezentseva, Galina Alikina, Anton Lukashevich, Vitalii Muzykantov, Rimma Bunina, Andrei Boronin, Egor Pazhetnov, Eugenii Paukshtis, Vladimir Kriventsov, Alevtina Smirnova, Oleksandr Vasylyev, John Irvine, Oleg Bobrenok, Vladimir Voronin, and Ivan Berger, Doped Nanocrystalline Pt-Promoted Ceria-Zirconia as Anode Catalysts for IT SOFC: Synthesis and Properties, Mater. Res. Soc. Symp. Proc. 1023 (2007) JJ02-07 1-6.

[27] L.G. Pinaeva, E.M. Sadovskaya, Yu.A. Ivanova, T.G. Kuznetsova, I.P. Prosvirin, V.A. Sadykov, Y. Schuurman, A.C. van Veen, C. Mirodatos, Water gas shift and partial oxidation of CH_4 over CeO_2–ZrO_2(–La_2O_3) and Pt/CeO_2–ZrO_2(–La_2O_3): Performance under transient conditions, Chem. Eng. J. 257 (2014) 281–291.

[28] N.N. Sazonova, S.N. Pavlova, S.A. Pokrovskaya, N.A. Chumakova, V.A. Sadykov, Structured reactor with a monolith catalyst fragment for kinetic studies, Structured reactor with a monolith catalyst fragment for kinetic studies. The case of CH_4 partial oxidation on LaNiPt-catalyst, Chem. Eng. J. 154 (2009) 17-24.

[29] S.N. Pavlova, N.N. Sazonova, V.A. Sadykov, G.M. Alikina, A.I. Lukashevich, E. Gubanova, R.V. Bunina, Study of synthesis gas production over structured catalysts based on LaNi(Pt)Ox- and Pt(LaPt)-CeO_2-ZrO_2 supported on corundum, Stud. Surf. Sci. Catal. 167 (2007) 343-348.

[30] I. Tavazzi, A. Beretta, G. Groppi, P. Forzatti, Development of a molecular kinetic scheme for methane partial oxidation over a Rh/α-Al_2O_3 catalyst, J. Catal. 241 (2006) 1–13.

[31] G.I. Marchuk, V.V. Shaidurov, Difference Methods and Their Extrapolations. Springer, New York, 1983.

[32] V. Sadykov, V. Sobyanin, N. Mezentseva, G. Alikina, Z. Vostrikov, Y. Fedorova, V. Pelipenko, V. Usoltsev, S. Tikhov, A. Salanov, L. Bobrova, S. Beloshapkin, J.R.H. Ross, O. Smorygo, V. Ulyanitskii, V. Rudnev, Transformation of CH_4 and liquid fuels into syngas on monolithic catalysts, Fuel 89 (2010) 1230–1240.

[33] V. Sadykov, L. Bobrova, S. Pavlova, V. Simagina, L. Makarshin, V. Parmon, J.R.H. Ross, A.C. van Veen, C. Mirodatos. Syngas Generation from Hydrocarbons and Oxygenates with Structured Catalysts. Series Energy Science, Engineering and technology, Nova Science Publishers, Inc, New York, 2012, 140 p, ISBN: 978-1-60876-323-8.

[34] G.F. Froment, K.B. Bischoff, J. De Wilde, Chemical Reactor Analysis and Design, John Wiley & Sons, Inc., Hoboken, 2011.

[35] O.P. Klenov, S.A. Pokrovskaya, N.A. Chumakova, S.N. Pavlova, V.A. Sadykov, A.S. Noskov, Effect of mass transfer on the reaction rate in a monolithic catalyst with porous walls, Catalysis Today 144 (2009) 258–264.

[36] M. Fathi, E. Bjorgum, T. Viig, O.A. Rokstad, Partial oxidation of methane to synthesis gas: Elimination of gas phase oxygen, Catalysis Today 63 (2000) 489–497.

[37] C. Batiot-Dupeyrat, G. Valderrama, A. Meneses, F. Martinez, J. Barrault, J.M. Tatibouet, Pulse study of CO_2 reforming of methane over $LaNiO_3$, Applied Catalysis A: General 248 (2003) 143–151.

[38] A. Slagtern, Y. Schuurman, C. Leclercq, X. Verykios, C. Mirodatos, Specific features concerning the mechanism of methane reforming by carbon dioxide over Ni/La_2O_3 catalyst, J. Catal. 172 (1997) 118–126.

[39] M. García-Diéguez, I.S. Pieta, M.C. Herrera, M.A. Larrubia, I. Malpartida, L.J. Alemany, Transient study of the dry reforming of methane over Pt supported on different γ-Al_2O_3, Catal. Today 149 (2010) 380–387.

[40] A. Horváth, G. Stefler, O. Geszti, A. Kienneman, A. Pietraszek, L. Guczi, Methane dry reforming with CO_2 on CeZr-oxide supported Ni, NiRh and NiCo catalysts prepared by sol–gel technique: Relationship between activity and coke formation**,** Catalysis Today 169 (2011) 102–111.

[41] J.A. Montoya, E. Romero-Pascual, C. Gimon, P. Del Angel, A. Monzón, Methane reforming with CO_2 over Ni/ZrO_2–CeO_2 catalysts prepared by sol–gel, Catalysis Today 63 (2000) 71–85.

[42] M. Rezaei, S.M. Alavi, S. Sahebdelfar, P. Bai, X. Liu, Z.-F. Yan, CO_2 reforming of CH_4 over nanocrystalline zirconia-supported nickel catalyst, Applied Catalysis B: Envir. 77 (2008) 346–354.

[43] V.A. Sadykov, S.N. Pavlova, R.V. Bunina, G.M. Alikina, S.F. Tikhov, T.G. Kuznetsova, Yu.V. Frolova, A.I. Lukashevich, O.I. Snegurenko, N.N. Sazonova, E.V. Kazantseva, Yu.N. Dyatlova, V.V. Usol'tsev, I.A. Zolotarskii, L.N. Bobrova, V.A. Kuz'min, L.L. Gogin, Z.Yu. Vostrikov, Yu.V. Potapova, V.S. Muzykantov, E.A. Paukshtis, E.B. Burgina, V.A. Rogov, V.A. Sobyanin, V.N. Parmon, Selective oxidation of hydrocarbons into synthesis gas at short contact times: Design of monolith catalysts and main process parameters, Kinetics and Catalysis 46, No. 2 (2005) 227–250.

Figure Captions

Fig. 1. Effluent concentrations of reactants A (*a*, *b*) and O_2 (*c*) as well as surface oxygen coverage θ by the [ZO] species (*d*) versus time at different rates of oxygen bulk diffusion: D_V = 10^{-19} (curves 1), 10^{-14} (curves 2), and 10^{-10}cm^2/s (curves 3). τ = 0.03 s, c^{in}_{O2} = 1.5 %, c^{in}_{A} = 3.0 %, k_1 = k_2 = 20 s^{-1}.

Fig. 2. Effluent concentrations in step-up transient experiments using a feed of 7% CH_4 and 7% CO_2 at 750 °C and contact times of 4.7 (*a*), 8 (*b*), and 15 ms (*c*).

Fig. 3. Transient traces of CH_4 (*a*) and CO_2 (*b*) reactant concentrations in the effluent for D_V = 10^{-13} cm^2/s and β = 0.2 (curves 1), D_V = 2.5·10^{-13} cm^2/s and β = 0.2 (curves 2), and D_V = 2.5·10^{-13} cm^2/s and β = 0.4 (curves 3). T = 750 °C, τ = 4.7 ms, c^{in}_{CH4} = 7 %, c^{in}_{CO2} = 7 %, k_1 = 80 s^{-1}, k_2 = 180 s^{-1}, k_{-2} = 260 s^{-1}, k$_3$ = 60 s^{-1}, and α = 0.04.

Fig. 4. Transients of the concentrations of the surface species [ZO] (*a*) and subsurface oxygen θ_V (*b*) for the case shown in Fig. 3 (curves 2).

Fig. 5. Experimental data (points) versus calculated curves for CH_4 and CO_2 reactant concentrations at the reactor outlet for the contact time 4.7 ms and parameters for the case 2 in Fig. 3.

Fig. 6. Influence of the oxygen diffusion D_V on the transient behavior of the surface fractions of [ZO] *(a)* and [ZCO$_3$] (*b*) at the reactor outlet: D_V = 1.0·10^{-13} (curves 1), 2.5·10^{-13} (curves 2), and 4.0·10^{-13} cm^2/s (curves 3). T=750°C, τ = 4.7 ms, c^{in}_{CH4} = 7 %, c^{in}_{CO2} = 7 %, k_1 = 200 s^{-1}, k_{-1} = 0.6 s^{-1}, k_2 = 550 s^{-1}, k_3 = 60 s^{-1}, k_4 = 315 s^{-1}, k_{-4} = 5 s^{-1}, k_5 = 60 s^{-1}, k_6 = 110 s^{-1}, α = 0.04, and β = 0.20.

Fig. 7. Influence of the oxygen diffusion D_V on the transient behavior of the subsurface oxygen fraction θ_V at the reactor outlet for the cases shown in Fig. 6: $D_V = 1.0 \cdot 10^{-13}$ (case 1, plot *a*), $2.5 \cdot 10^{-13}$ (case 2, plot *b*) [16] and $4.0 \cdot 10^{-13}$ cm^2/s (case 3, plot *c*). Other parameters are the same as reported in Fig. 6.

Fig. 8. Influence of the oxygen diffusion D_V on the transient behavior of the reagent concentrations c_{CH4} (plots *a* and *c*) and c_{CO2} (plots *b* and *d*) at the reactor outlet for the cases presented in Fig.6: $D_V = 1.0 \cdot 10^{-13}$ (curves 1), $2.5 \cdot 10^{-13}$ (curves 2), and $4.0 \cdot 10^{-13}$ cm^2/s (curves 3). Other parameters are the same as reported in Fig. 6.

Fig. 9. Influence of the oxygen diffusion D_V on the transient behavior of the product concentrations c_{CO} (*a*) and c_{H2} (*b*) at the reactor outlet for the cases in Fig. 6: $D_V = 1.0 \cdot 10^{-13}$ (curves 1), $2.5 \cdot 10^{-13}$ (curves 2), and $4.0 \cdot 10^{-13}$ cm^2/s (curves 3). Other parameters are the same as reported in Fig. 6.

Fig. 10. Comparison of the experimental data (points) and model predictions (solid lines) for the concentrations of CH_4 (plots *a* and *c*) and CO_2 (plots *b* and *d*) in the effluent at different contact times $\tau = 4.7$ and 8 ms (*a* and *b*) and $\tau = 15$ ms (*c* and *d*). T = 750 °C, $c^{in}_{CH4} = 7$ %, $c^{in}_{CO2} = 7$ %, $k_1 = 220$ s^{-1}, $k_{-1} = 0.6$ s^{-1}, $k_2 = 550$ s^{-1}, $k_3 = 60$ s^{-1}, $k_4 = 315$ s^{-1}, $k_{-4} = 5$ s^{-1}, $k_5 = 60$ s^{-1}, $k_6 = 110$ s^{-1}, $\alpha = 0.04$, and $\beta = 0.20$.

Fig. 11. Comparison of the experimental data (points) and calculated curves (solid lines) for the concentrations of CO (plot *a*) and H_2 (plot *b*) in the effluent at different contact times $\tau = 4.7$ ms and $\tau = 8$ ms. Other parameters correspond to those reported in Fig. 10.

Table

Table 1. 6-stage reaction mechanism

№	Catalytic stages	Routes		
		I	II	III
1	$CO_2 + [ZO] \leftrightarrow [ZCO_3]$	1		
2	$CH_4 + [ZCO_3] \rightarrow 2\,CO + 2\,H_2 + [ZO]$	1		
3	$CH_4 + [ZO] \rightarrow CO + 2\,H_2 + [Z]$		1	
4	$[Z] + [Os] \leftrightarrow [ZO] + [Vs]$		1	1
5	$CO_2 + [Vs] \rightarrow CO + [Os]$		1	1
6	$H_2 + [ZO] \rightarrow H_2O + [Z]$			1

№	Routes
I	$CH_4 + CO_2 \leftrightarrow 2\,CO + 2\,H_2$
II	$CH_4 + CO_2 \leftrightarrow 2\,CO + 2\,H_2$
III	$CO_2 + H_2 \leftrightarrow CO + H_2O$

Figure

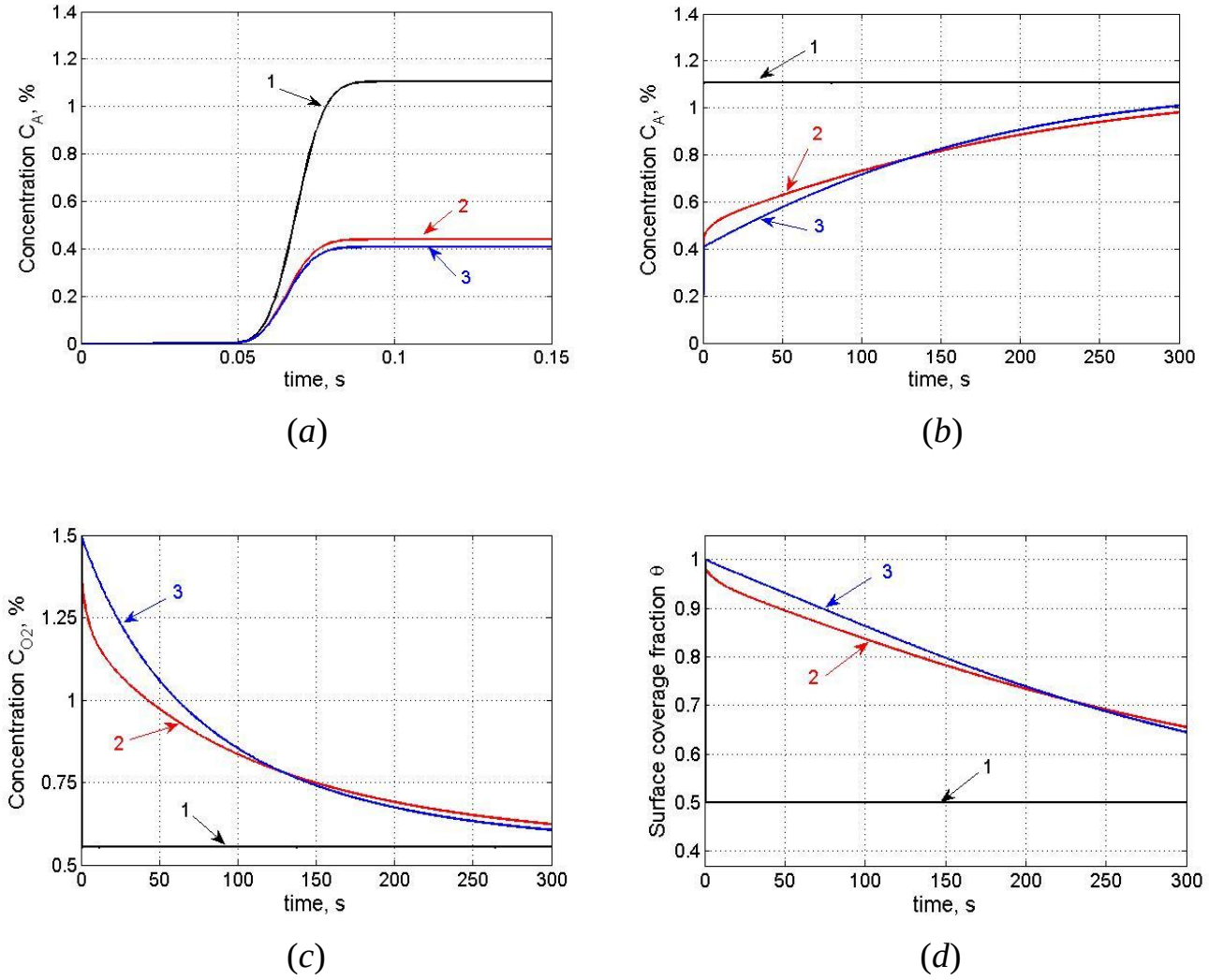

Fig. 1. Effluent concentrations of reactants A (*a*, *b*) and O_2 (*c*) as well as surface oxygen coverage θ by the [ZO] species (*d*) versus time at different rates of oxygen bulk diffusion: $D_V = 10^{-19}$ (curves 1), 10^{-14} (curves 2), and 10^{-10} cm^2/s (curves 3). $\tau = 0.03$ s, $c^{in}_{O2} = 1.5$ %, $c^{in}_{A} = 3.0$ %, $k_1 = k_2 = 20$ s^{-1}.

Figure

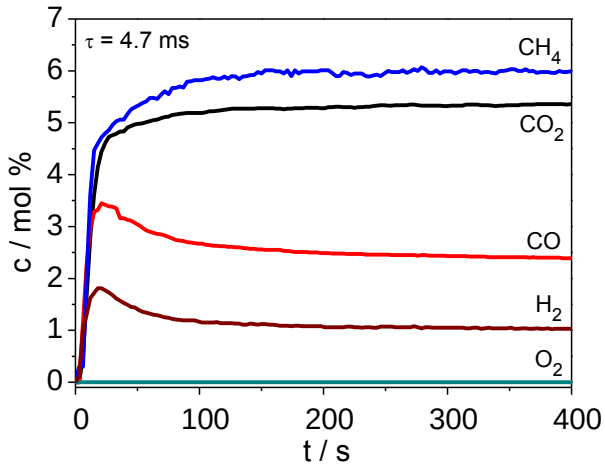

(*a*)

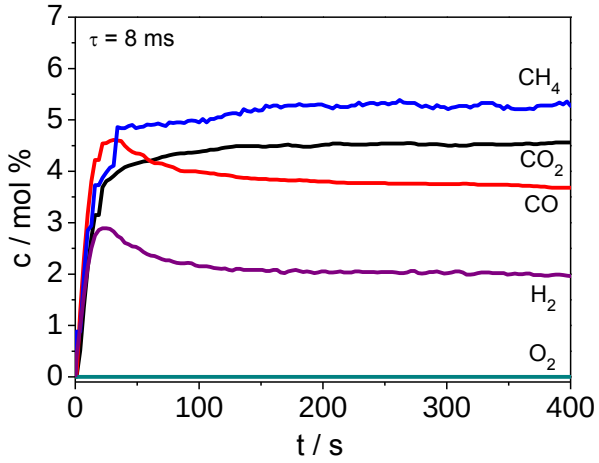

(*b*)

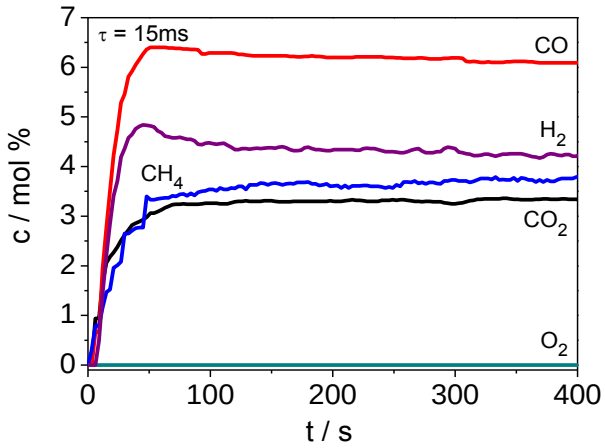

(*c*)

Fig. 2. Effluent concentrations in step-up transient experiments using a feed of 7% CH_4 and 7% CO_2 at 750 °C and contact times of 4.7 (*a*), 8 (*b*), and 15 ms (*c*).

Figure

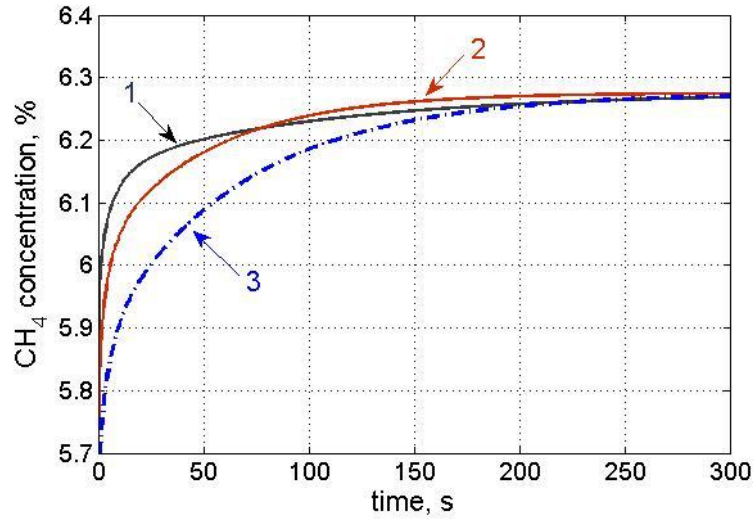

(*a*)

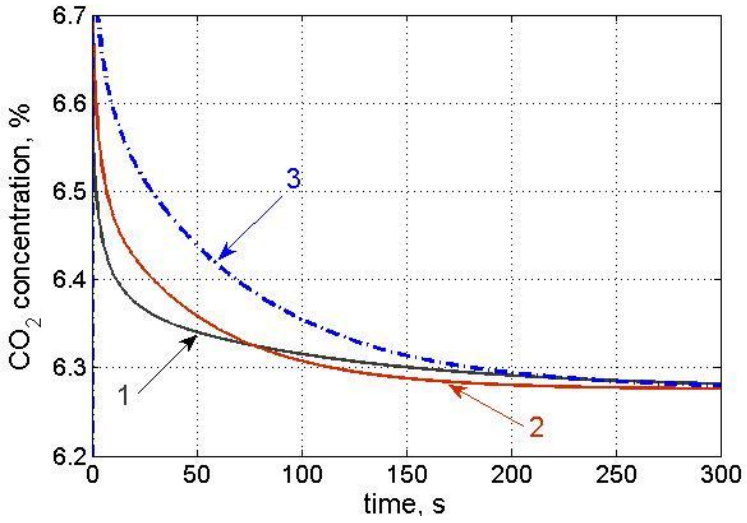

(*b*)

Fig. 3. Transient traces of CH_4 (*a*) and CO_2 (*b*) reactant concentrations in the effluent for D_V = 10^{-13} cm^2/s and β = 0.2 (curves 1), D_V = 2.5·10^{-13} cm^2/s and β = 0.2 (curves 2), and D_V = 2.5·10^{-13} cm^2/s and β = 0.4 (curves 3). T = 750 °C, τ = 4.7 ms, c^{in}_{CH4} = 7 %, c^{in}_{CO2} = 7 %, k_1 = 80 s^{-1}, k_2 = 180 s^{-1}, k_{-2} = 260 s^{-1}, k_3 = 60 s^{-1}, and α = 0.04.

Figure

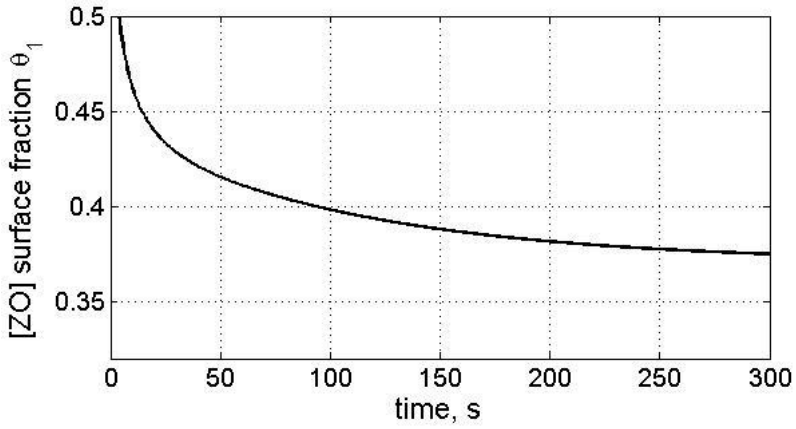

(*a*)

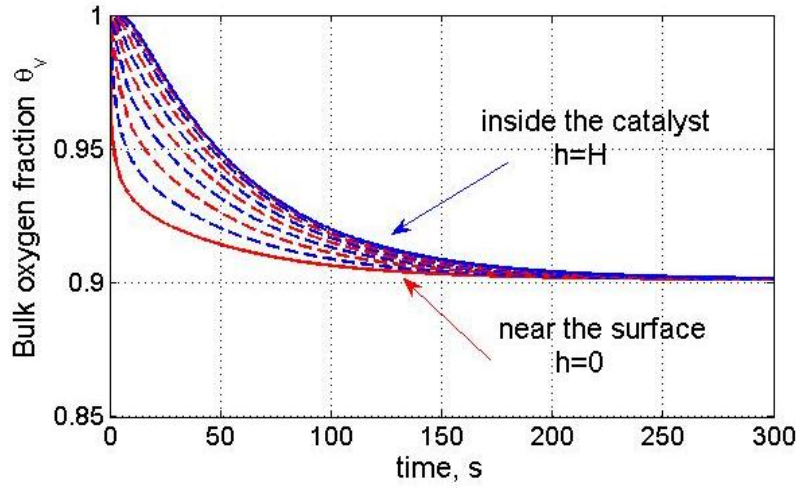

(*b*)

Fig. 4. Transients of the concentrations of the surface species [ZO] (*a*) and subsurface oxygen θ_V (*b*) for the case shown in Fig. 3 (curves 2).

Figure

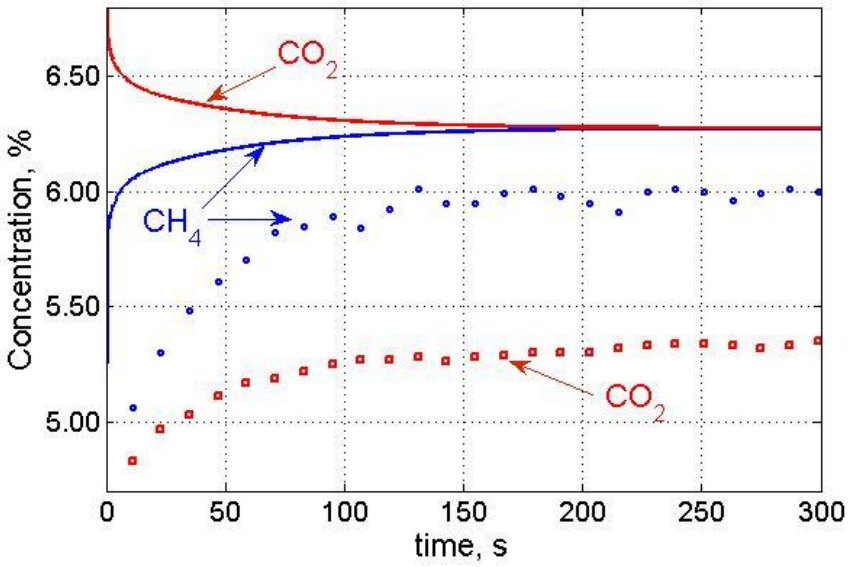

Fig. 5. Experimental data (points) versus calculated curves for CH_4 and CO_2 reactant concentrations at the reactor outlet for the contact time 4.7 ms and parameters for the case 2 in Fig. 3.

Figure

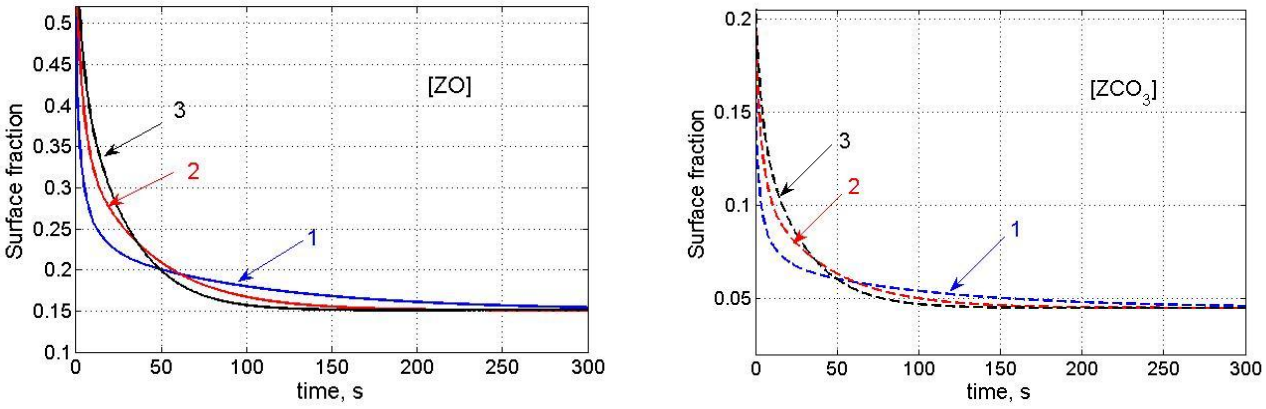

(*a*) (*b*)

Fig. 6. Influence of the oxygen diffusion D_V on the transient behavior of the surface fractions of [ZO] *(a)* and [ZCO_3] (*b*) at the reactor outlet: $D_V = 1.0 \cdot 10^{-13}$ (curves 1), $2.5 \cdot 10^{-13}$ (curves 2), and $4.0 \cdot 10^{-13}$ cm^2/s (curves 3). T=750°C, τ = 4.7 ms, c^{in}_{CH4} = 7 %, c^{in}_{CO2} = 7 %, k_1 = 200 s^{-1}, k_{-1} = 0.6 s^{-1}, k_2 = 550 s^{-1}, k_3 = 60 s^{-1}, k_4 = 315 s^{-1}, k_{-4} = 5 s^{-1}, k_5 = 60 s^{-1}, k_6 = 110 s^{-1}, α = 0.04, and β = 0.20.

Figure

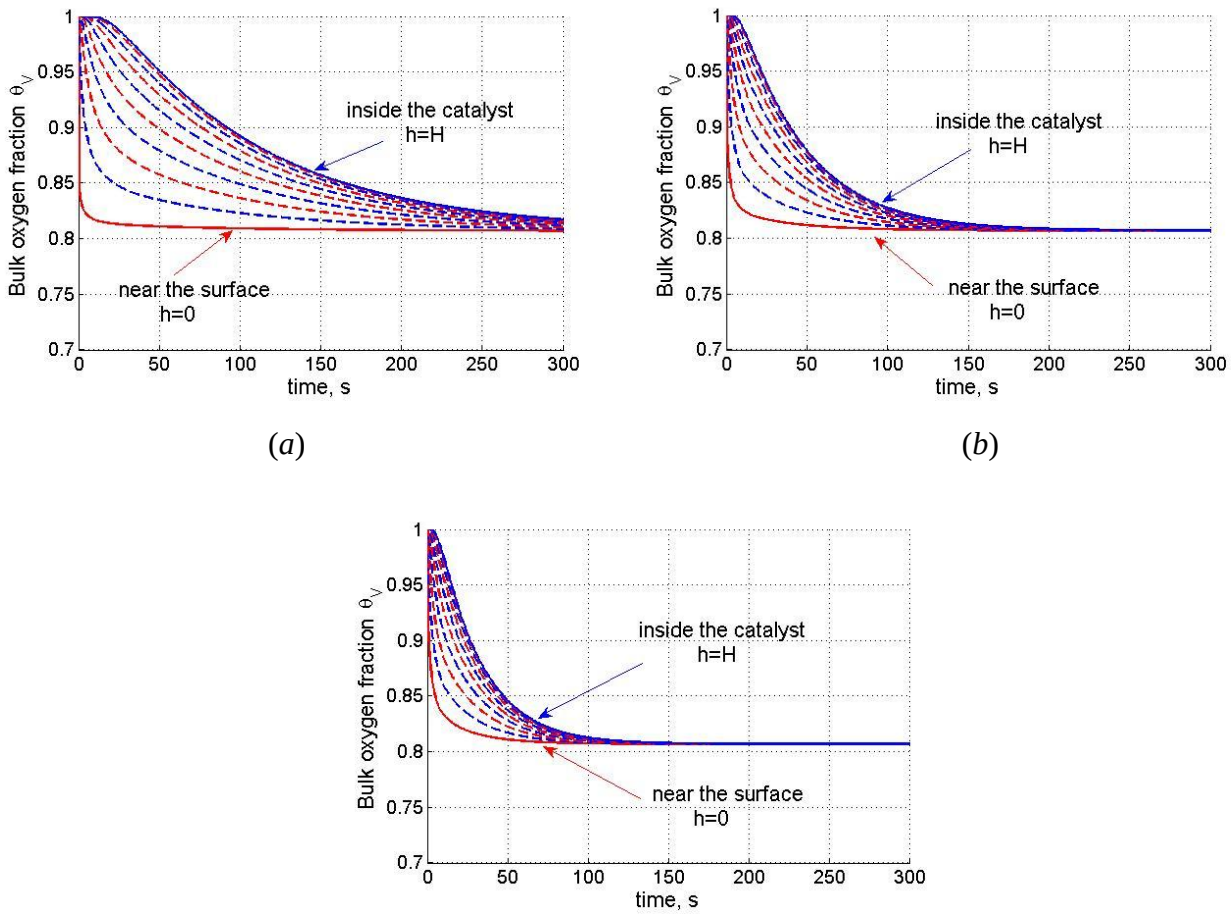

Fig. 7. Influence of the oxygen diffusion D_V on the transient behavior of the subsurface oxygen fraction θ_V at the reactor outlet for the cases shown in Fig. 6: $D_V = 1.0 \cdot 10^{-13}$ (case 1, plot *a*), $2.5 \cdot 10^{-13}$ (case 2, plot *b*) [16] and $4.0 \cdot 10^{-13}$ cm^2/s (case 3, plot *c*). Other parameters are the same as reported in Fig. 6.

Figure

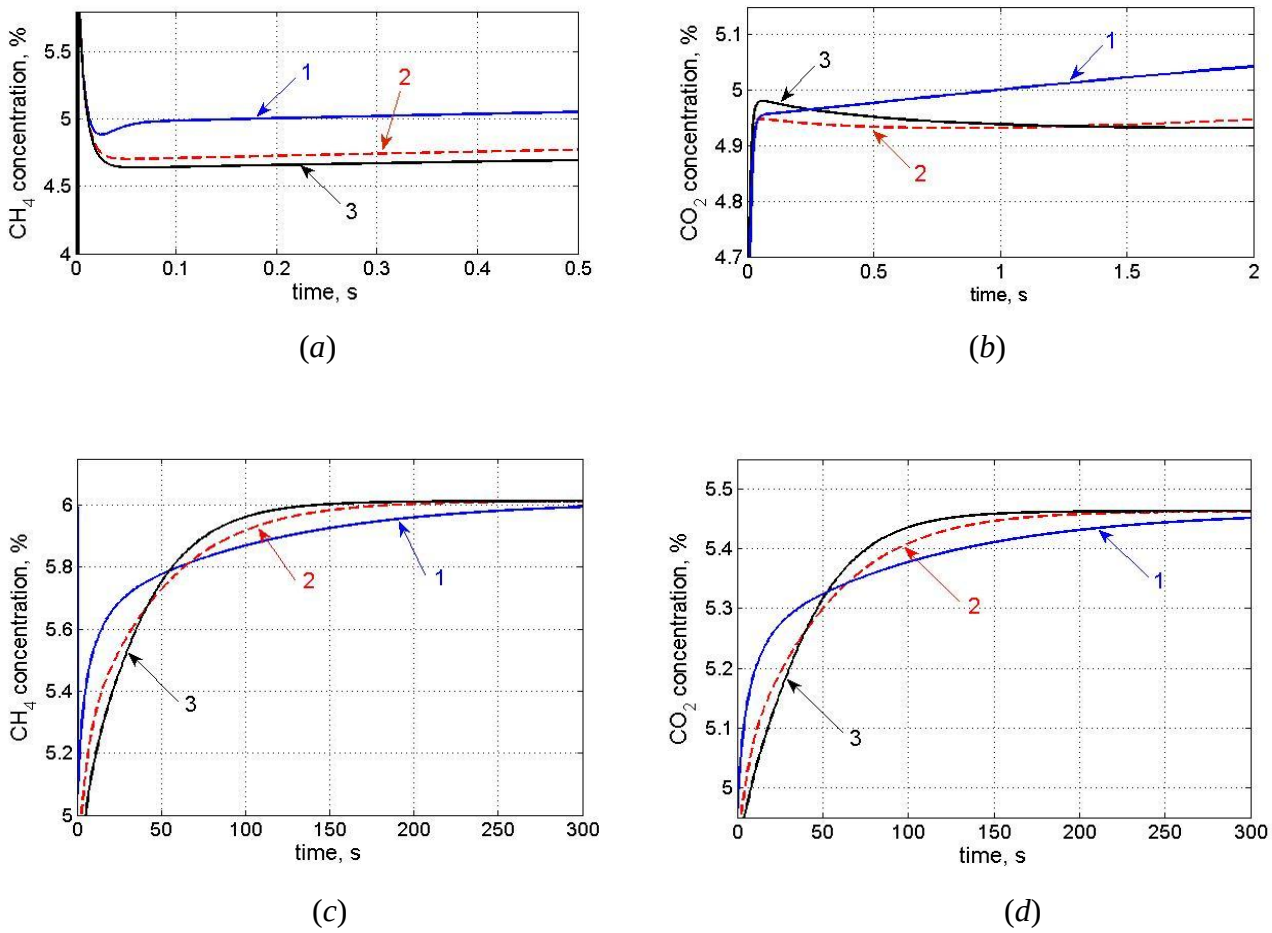

Fig. 8. Influence of the oxygen diffusion D_V on the transient behavior of the reagent concentrations c_{CH4} (plots *a* and *c*) and c_{CO2} (plots *b* and *d*) at the reactor outlet for the cases presented in Fig.6: $D_V = 1.0 \cdot 10^{-13}$ (curves 1), $2.5 \cdot 10^{-13}$ (curves 2), and $4.0 \cdot 10^{-13}$ cm^2/s (curves 3). Other parameters are the same as reported in Fig. 6.

Figure

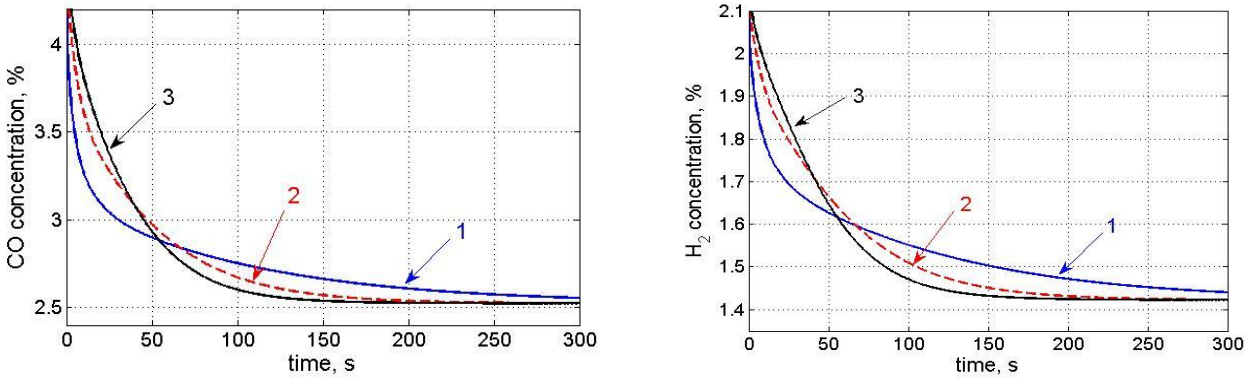

(*a*) (*b*)

Fig. 9. Influence of the oxygen diffusion D_V on the transient behavior of the product concentrations c_{CO} (*a*) and c_{H2} (*b*) at the reactor outlet for the cases in Fig. 6: $D_V = 1.0 \cdot 10^{-13}$ (curves 1), $2.5 \cdot 10^{-13}$ (curves 2), and $4.0 \cdot 10^{-13}$ cm^2/s (curves 3). Other parameters are the same as reported in Fig. 6.

Figure

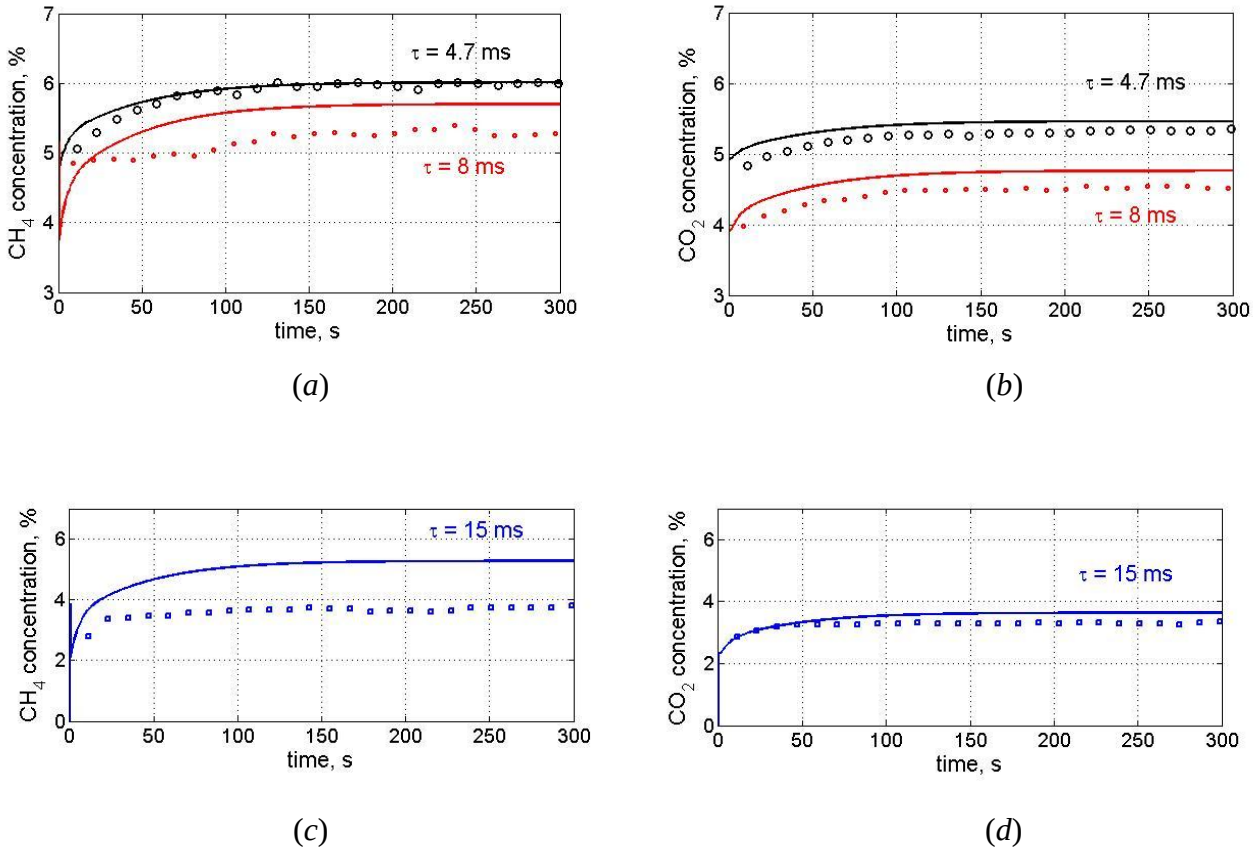

Fig. 10. Comparison of the experimental data (points) and model predictions (solid lines) for the concentrations of CH_4 (plots *a* and *c*) and CO_2 (plots *b* and *d*) in the effluent at different contact times τ = 4.7 and 8 ms (*a* and *b*) and τ = 15 ms (*c* and *d*). T = 750 °C, c^{in}_{CH4} = 7 %, c^{in}_{CO2} = 7 %, k_1 = 220 s^{-1}, k_{-1} = 0.6 s^{-1}, k_2 = 550 s^{-1}, k_3 = 60 s^{-1}, k_4 = 315 s^{-1}, k_{-4} = 5 s^{-1}, k_5 = 60 s^{-1}, k_6 = 110 s^{-1}, α = 0.04, and β = 0.20.

Figure

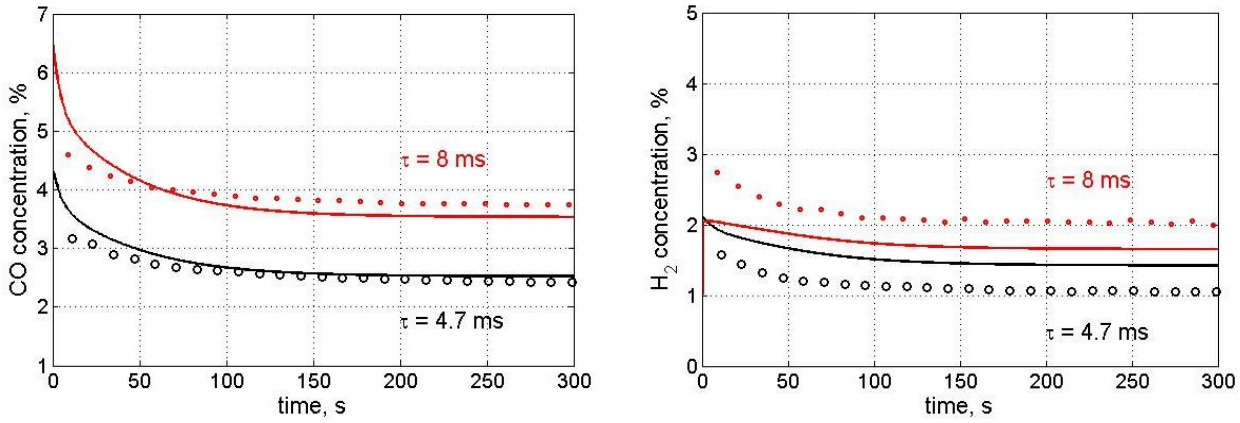

(*a*) (*b*)

Fig. 11. Comparison of the experimental data (points) and calculated curves (solid lines) for the concentrations of CO (plot *a*) and H_2 (plot *b*) in the effluent at different contact times τ = 4.7 ms and τ = 8 ms. Other parameters correspond to those reported in Fig. 10.